Potential impact of aerosols on convective clouds revealed by Himawari-8 observations over different terrain types in eastern China

Tianmeng Chen[a,b,c], Zhanqing Li[b,*], Ralph A. Kahn[b,d], Chuanfeng Zhao[a,*], Daniel Rosenfeld[e], Jianping Guo[c], Wenchao Han[a,bf], Dandan Chen[c]

a. State Key Laboratory of Remote Sensing Sciences, and College of Global Change and Earth System Science, Beijing Normal University, Beijing, 100875, China

b. Department of Atmospheric and Oceanic Sciences & Earth System Science Interdisciplinary Center, University of Maryland, College Park, Maryland 20740, USA

c. State Key Laboratory of Severe Weather, Chinese Academy of Meteorological Sciences, Beijing 100081, China

d. Earth Sciences Division, NASA Goddard Space Flight Center, Greenbelt, Maryland 20771 USA

e. Institute of Earth Sciences, Hebrew University, Jerusalem, Israel

f. Chinese Research Academy of Environmental Sciences, Beijing, 100012, China

* To whom all correspondence should be addressed

Zhanqing Li

  Email: zli@atmos.umd.edu

Chuanfeng Zhao

  Email: czhao@bnu.edu.cn

Abstract

Convective clouds are common and play a major role in Earth's water cycle and energy balance; they may even develop into storms and cause severe rainfall events. To understand the convective cloud development process, this study investigates the impact of aerosols on convective clouds by considering the influence of both topography and diurnal variation of radiation. By combining texture analysis, clustering and thresholding methods, we identify all convective clouds in two warm seasons (May-September, 2016-2017) in eastern China based on Himawari-8 Level 1 data. Having a large diurnally resolved cloud data together with surface meteorological and environmental measurements, we investigate convective cloud properties and their variation, stratified by elevation and diurnal change. We then analyze the potential impact of aerosol on convective clouds under different meteorological conditions and topographies. In general, convective clouds tend to occur preferentially under polluted conditions in the morning, which reverses in the afternoon. Convective cloud fraction first increases then decreases with aerosol loading, which may contribute to this phenomenon. Topography and diurnal meteorological variations may affect the strength of aerosol microphysical and radiative effects. Updraft is always stronger along the windward slopes of mountains and plateaus, especially in northern China. The prevailing southerly wind near the foothills of mountains and plateaus is likely to contribute to this windward strengthening of updraft and to bring more pollutant into the mountains, thereby strengthening the microphysical effect, invigorating convective clouds. By comparison, over plain, aerosols decrease surface heating and suppresses convection by blocking solar radiation reaching the surface.

Key Words

Himawari-8; convective cloud; aerosol-cloud interactions, topographic effects on cloud

1. Introduction

Convective clouds are important for Earth's energy balance and the water cycle. Changes in the distribution or triggering time of convective cloud can have a large impact on the climate system (Stocker et al., 2013). Previous studies have shown that aerosol particles in the atmosphere can affect the formation and development of convective clouds, through both radiative and microphysical effects (Ramanathan et al., 2001;Tao et al., 2012;Altaratz et al., 2014;Rosenfeld et al., 2014a;2014b;Li et al., 2016;Zhao et al., 2018a;Yang et al., 2019), which can dramatically affect the weather and climate (Zhao et al., 2020).

Aerosol particles generally cool the surface by scattering the downward solar radiation (McCormick and Ludwig, 1967;Charlson et al., 1992), whereas light-absorbing aerosols can additionally warm the atmosphere above the surface (Ackerman et al., 2000). These aerosol radiative effects change the surface radiation budget and the atmospheric temperature profile directly, thereby altering the onset time of convective cloud formation and precipitation (Feingold et al., 2005;Wang et al., 2013;Zhou et al., 2020).

Aerosols, by acting as cloud condensation nuclei (CCN) and/or ice nuclei (IN), can also affect the formation and growth of cloud droplets (Rosenfeld, 2000;Kaufman et al., 2002;Garrett et al., 2004;Lohmann and Feichter, 2005;Zhao et al., 2012), which is regarded as the aerosol microphysical effect. For constant cloud liquid water content, increases in aerosol particle number concentration can produce more but smaller cloud droplets, thus increasing cloud albedo (Twomey and Warner, 1967;Twomey, 1974). This effect, called the "Twomey effect", is a well-established influence on cloud properties in polluted environments (Kaufman and Nakajima, 1993;Feingold et al., 2003). Smaller cloud droplets can increase cloud lifetime and reduce precipitation (Albrecht, 1989), whereas for some deep convective cloud, the latent heat released by the formation of more and smaller ice particles can invigorate deep convection and

76   increase rain rate (Andreae et al., 2004;Kaufman et al., 2005;Rosenfeld et al., 2008;Li

77   et al., 2011;Fan et al., 2013;Li et al., 2019). Koren et al. (2005) also found an increase

78   in cloud fraction with a decrease in cloud top pressure for clouds under high aerosol

79   loading environment. For cases of thin clouds, smaller cloud droplets enhance cloud

80   thermal emissivity, trap more longwave radiation within the atmosphere and alter cloud

81   development (Garrett and Zhao, 2006;Zhao and Garrett, 2015).

82   Many previous studies show that the interactions between aerosols and weather

83   variables are complex (Williams et al., 2002;Stevens and Feingold, 2009;Altaratz et al.,

84   2014), making it challenging to untangle aerosol effects from meteorological factors

85   that influence convective clouds. As different types of clouds form under different

86   meteorological conditions, some previous observational studies attempted to classify

87   clouds into different types, to distinguish aerosol effects in various meteorological

88   regimes (Andreae et al., 2004;Khain et al., 2005;Li et al., 2011;Gryspeerdt and Stier,

89   2012;Gryspeerdt et al., 2014;Qiu et al., 2017). Other studies consider different cloud

90   types as different stages of convective development, to identify aerosol effects on

91   convective cloud evolution, stratified by meteorological conditions (Chen et al.,

92   2016;Guo et al., 2018).

93   Meteorological conditions can change during the day and can vary from one place to

94   another. For example, convective cloud and precipitation maxima tend to occur in the

95   early morning over open ocean, but in the late afternoon or early evening over land,

96   driven primarily by temporal differences in the radiative forcing (Chang et al.,

97   1995;Garreaud and Wallace, 1997;Sui et al., 1997;Zhou et al., 2008;Li et al., 2010).

98   Other studies show that the impact of terrain on the convective cloud can also be

99   complex (Roe, 2005;Houze Jr., 2012), and that the meteorological factors that control

100   convection can be affected by terrain (Romatschke and Jr., 2010, 2011a, b). Diurnal

101   variation of solar radiation can alter wind circulation in a valley, and therefore may

102   control the spatial distribution of convective cloud in mountainous regions (Kirshbaum

103   and Durran, 2004, 2005;Kirshbaum et al., 2007;Romatschke et al., 2010).

104   Studies also attempted to explore the effects of topography on
105   aerosol-precipitation interactions. Lynn et al. (2007) simulated the aerosol effect on
106   orographic precipitation using the Weather Research and Forecasting Model (WRF)
107   and found that the intensity of orographic precipitation is suppressed in
108   more polluted environments. However, when the cold rain process is involved,
109   precipitation is delayed but intensified (Givati and Rosenfeld, 2004;Rosenfeld and
110   Givati, 2006;Xiao et al., 2015;Yang et al., 2016c) When light-absorbing aerosol is
111   present, radiative heating in the atmosphere can produce enhanced instability, which
112   may trigger disastrous precipitation, especially late in the day (Fan et al., 2015). These
113   studies revealed some potential influences of aerosol on orographic precipitation from
114   either model-simulations or from several specific observed cases. Only a few studies
115   include long-term observational data to analyze the relationships between
116   aerosol and orographic precipitation statistically (Rosenfeld,
117   2007;Guo et al., 2014). This might be due to a lack of observational data in the past
118   with sufficiently high spatial and temporal resolution.

119   ~~Although p~~Tracking the development of convective cloud can provide more details
120   of changes in cloud lifecycle.~~olar orbiting satellites provide high spatial resolution data,~~
121   ~~Studies such as~~ ~~Meskhidze et al. (2009),~~ ~~A~~attempts have been made~~ed~~ to
122   ~~explored~~investigate differences in cloud properties between ~~the~~ morning~~-~~ ~~to~~and
123   afternoon ~~cloud property changes~~ using Terra and Aqua MODIS data (e.g. Meskhidze
124   et al., 2009), but they cannot track the ~~diurnal~~ development of convective clouds beyond
125   two snapshots per day. ~~In~~ On the ~~contrast~~contrary, geostationary satellite data can
126   provide images every 2.5-15 minutes, making it possible to track the evolution of
127   convective clouds individually over the entire day ~~at a slightly lower spatial resolution~~
128   (Chakraborty et al., 2015;Chakraborty et al., 2016). The launch of the Japanese next-
129   generation geostationary satellite Himawari-8 in October 2014 rendered an opportunity
130   to study aerosol effects on convective clouds throughout the day. The diurnal variation
131   in different terrain types may be particularly strong due to amplified variations in

radiation and sunshine duration by terrain (Li and Weng, 1987, 1988, 1989). The current study aims to characterize the differences between convective clouds in polluted and clean environments, untangling the ~~probable~~potential influence of topography on the way aerosols affect convective clouds, and to explore how the effects of aerosols change diurnally. To achieve this goal, we first develop an automatic method of identifying convective clouds using geostationary satellite data, and then assess how aerosol effects change during the day and in different topographic regions of eastern China.

The paper is organized as follows: Section 2 introduces the study region and data selection. The method is described in Section 3. Section 4 presents the temporal and spatial distributions of convective cloud and discusses the possible impact by aerosol on convective cloud over different terrains. In section 5, we give a brief summary.

2. Study region and data

2.1 Region of interest

Rapid economic and industrial growth has brought heavy pollution to China, especially to eastern China, in recent decades. Thus, high aerosol loading over this area provides a natural laboratory for us to study the aerosol impact on convective clouds (Guo et al., 2011). In addition, eastern China has relatively complex topography, where convective clouds can be triggered and develop differently, leading to convective cloud regimes having distinctive diurnal change patterns. In order to investigate the joint impact of aerosol pollution and topography on convective cloud fraction and diurnal variation, we chose the area ~~within~~of longitudes 105°E to 125°E, and latitudes 20°N to 45°N as the region of interest (ROI) for this study. We show the terrain distribution and the mean concentration of particles with aerodynamic diameters smaller than 2.5 μm (PM$_{2.5}$) during May-September in 2016-2017 over ~~eastern China~~ the ROI in eastern China in Figure 1. Generally, terrain height (TH) tends to increase from east to west in this region, and PM$_{2.5}$ mass concentration is generally higher over the plains and lower over mountain ranges and plateaus. ~~In order to investigate how these landscapes~~

159 ~~impact cloud fraction and convective cloud diurnal variation, we chose the area with~~
160 ~~longitudes from 105°E to 125°E, and latitudes from 20°N to 45°N as the region of~~
161 ~~interest (ROI) for this study.~~As PM$_{2.5}$ observations are available only over land in this
162 area, the aerosol-convective-cloud relationship is only discussed over land in this study.

2.2 Data

a. Himawari-8 data

The first in a new generation of Japanese geostationary meteorology satellite, named Himawari-8, was launched in 2014. It carries a state-of-art optical sensor, the Advanced Himawari Imager (AHI), which can provide significantly high resolution observations of the Earth system from space (0.5 or 1 km for visible and near-infrared bands at the sub-spacecraft point and 2 km for infrared bands) and time (around 10 min for Full Disk and 2.5 min for sectored regions) from space (Bessho et al., 2016). These advantages make it possible to detect rapid weather changes, especially the triggering and development of convective cloud. The geostationary sub-spacecraft point is located at 140.7°E over the equator, so most of our ROI is covered.

In this study, we use the Himawari-8 L1 gridded data from the Japan Aerospace Exploration Agency (JAXA) P-Tree system to develop a convective cloud identification method and investigate how aerosols impact convective clouds over eastern China. This dataset is generated by the Earth Observation Research Center (JAXA/EORC) from Himawari Standard Data, with re-sampling to equal latitude-longitude grids. (For more detail, see https://www.eorc.jaxa.jp/ptree/userguide.html ; last accessed: Oct. 2018 .) The channels we use here are centered at 0.64 μm, 11.2 μm, and 12.4 μm, with a spatial resolution of 0.02°×0.02° and a temporal resolution of 10 min.

b. MODIS cloud mask

We use the MODIS/Aqua MYD35 cloud mask data (Wilson et al., 2014) to validate the convective cloud identification method developed here. Cloud mask data at 1 km

186 resolution (from the MYD35 Cloud_Mask product; web address:
187 https://modis.gsfc.nasa.gov/data/dataprod/mod35.php; last accessed: ~~Sep~~Dec. 20~~18~~20)
188 is used to compare with the near-simultaneous cloud identification result from our
189 method.

190 c. Particulate matter (PM) data

191 In previous studies, aerosol optical depth (AOD) (Andreae, 2009;Niu and Li,
192 2012;Wang et al., 2018), visibility (Chen et al., 2016), aerosol concentration with
193 diameters between 100 nm and 3 μm (Zhao et al., 2018b;Yang et al., 2019;Zhao et al.,
194 2019), and particulate matter up to 10 μm in diameter (PM_{10}) (Guo et al., 2016) were
195 used as proxies for cloud concentration nuclei (CCN). However, satellite AOD
196 retrievals can only be made in cloud-free conditions, near-cloud retrievals are
197 frequently influenced by cloud contamination (Li et al., 2009), and the value is always
198 influenced by the moisture of atmosphere (Boucher and Quaas, 2012). In addition,
199 remote-sensing methods cannot distinguish the part of the CCN size spectrum smaller
200 than about 0.05 μm from atmospheric gas molecules. On the other hand, particulate
201 matter can be measured from the surface or aircraft under all-sky conditions and can
202 provide dried particle masses which can minimize the influence of moisture on it.
203 Besides, as eastern China is under continuous emissions of newly formed particles and
204 precursor gases, particles tend to grow into nucleation-mode easily, forming CCN and
205 leading to activations. In addition, CCN concentrations are to some extent proportional
206 to aerosol loading (Andreae, 2009;Liu and Li, 2014). Zhang et al. (2019) found that the
207 CCN number concentration increases with the total aerosol number concentration and
208 PM during haze events. Particle size up to 10 μm may be much larger than the typical
209 scale of CCN, so particulate matter up to 1 μm (PM_1) or 2.5 μm ($PM_{2.5}$) in
210 diameter are more proper to serve as CCN proxies. Due to the limited
211 availability of PM_1 measurements in eastern China, we chose $PM_{2.5}$ as an indicator of
212 different CCN levels in the environment for this study.

213   Figure 1 also shows the mean value of PM$_{2.5}$ measured at 1205 ground-based stations

214   across eastern China during the warm months (May-September) in 2016-2017. The

215   average PM$_{2.5}$ mass concentration generally lies between 20 and 60 μg/m^3, with higher

216   values over the Beijing-Tianjin-Hebei region. Although not uniformly distributed, the

217   ground stations cover almost all regions in eastern China. Note that these stations

218   provide hourly observations of PM$_{10}$ and PM$_{2.5}$ concentrations.

219   d. ~~r~~Reanalysis

220   In order to assess the impact of meteorological factors on convective clouds, and to

221   analyze the dependence of aerosol ~~effects on~~ convective ~~-~~cloud ~~fraction~~ relationship

222   on meteorological conditions, we adopt meteorological variables from th~~e~~e fifth

223   generation ECMWF (European Centre of Midium-Range Weather Forecast) reanalysis

224   for the global climate and weather (ERA 5, web address:

225   https://cds.climate.copernicus.eu/cdsapp#!/dataset/reanalysis-era5-single-

226   levels?tab=overview; last accessed: Dec. 2020) and the second Modern-Era

227   Retrospective analysis for Research and Applications (MERRA-2) reanalysis dataset

228   (Gelaro et al., 2017) (web address: https://gmao.gsfc.nasa.gov/reanalysis/MERRA-2/;

229   last accessed: Oct. 2019). ~~MERRA-2 is the latest atmospheric reanalysis produced by~~

230   ~~NASA's Goddard Earth Observing System Data Assimilation System Version 5~~

231   ~~(GEOS-5), using a new generation of satellite observation sources from 1979 to the~~

232   ~~present (Gelaro et al., 2017). In this study, we adopt the temperature at 2 m, relative~~

233   ~~humidity at 700 hPa and 850 hPa, vertical velocity at 925 hPa and 850 hPa, and surface~~

234   ~~specific humidity t~~To evaluate how convective cloud fraction changes with respect to

235   terrain height under different meteorological conditions, and to gain insight into

236   whether the aerosol effects are independent of other factors that might influence

237   convective cloud triggering and development during daytime~~.~~. ~~We obtained all these~~

238   ~~parameters at a spatial resolution of 0.5°×0.5°, and a temporal resolution of 3 hours.~~

239   ~~Based on the findings in previous studies,~~ we chose the following factors to characterize

240   the dynamics and thermodynamics of the environment, all these parameters are

obtained at a spatial resolution of 0.5°×0.5°, and a temporal resolution of 3 hours.

Convective Available Potential Energy (CAPE). CAPE is adopted from the ERA 5 reanalysis dataset, which is calculated from the ECMWF Integrated Forecasting System (IFS), by considering parcels of air departing at different model levels below the 350 hPa level (Hersbach et al., 2018). Numerous studies have shown that CAPE is a good indicator of atmospheric instability (Williams et al., 2002), and can reflect the potential ability of convective clouds formation and development.

Potential Temperature. Temperature, especially lower-level atmospheric temperature,

Potential Temperature. Temperature, especially lower-level atmospheric temperature,

Potential Temperature. Temperature, especially lower-level atmospheric temperature,

Potential Temperature. Temperature, especially lower-level atmospheric temperature,

Potential Temperature. Temperature, especially lower-level atmospheric temperature,

Potential Temperature. Temperature, especially lower-level atmospheric temperature,

$$LTS = \theta_{700\,hPa} - \theta_{surface} \qquad (1)$$

$\theta_{surface}$, which represent the potential temperature at the surface, is calculated from the air temperature at 2 m; the potential temperature at 700 hPa ($\theta_{700\,hPa}$) is directly extracted from MERRA-2 pressure level dataset.

Potential Temperature. Temperature, especially lower-level atmospheric temperature, plays a critical role in triggering the development of convective clouds. As air temperature decreases systematically with altitude in most places, it is not proper to directly compare temperatures over different terrain. As the potential temperature is conserved regardless of height, it reflects the near-surface heating to some extent. Additionally, Wang et al. (2018) point out that selecting potential temperature avoids some duplication of temperature and humidity information. Thus, potential temperature is adopted, and we use the temperature at 2 m to calculate the near-surface potential temperature (θ) in this study.

267   *Vertical velocity*. Vertical velocities at 800 hPa (ω_{800}) and 900 hPa (ω_{900})

268 are chosen to investigate the role of vertical airflow in convection. As vertical motion

269 over different terrain may vary, this factor can produce large differences in convective

270 cloud occurrence frequency. We use ω_{800} and ω_{900} to represent the low-level

271 dynamical conditions for terrain above and below 1000 m, respectively, so that we can

272 roughly assess the ω about 1000m above the surface in these regions despite varying

273 terrain height. $\omega>0$ represents downward air motion, whereas $\omega<0$ means the air motion

274 is upward. Uncertainty lies in the different distances between the 800 hPa and

275 900 hPa level and cloud base. There are likely large differences in the updraft strength

276 between these two levels and the cloud bases in some cases. However, in the formation

277 of convective clouds, the vertical velocity between the surface and cloud base is more

278 essential in transporting vapor and energy to higher levels. As these two levels cover

279 most of the surfaces above and below 1000 m and can reflect the vertical velocities

280 beneath cloud to some extent, we chose to use them as reference values to represent the

281 dynamical conditions when convective clouds occur.

282   *Humidity*. Water vapor supply is essential to the formation and

283 development of convective clouds (Redelsperger et al., 2002;Chakraborty et al., 2018)

284 and is a crucial component of cloud water condensation and evaporation in aerosol-

285 cloud interactions (Altaratz et al., 2014). As convective cloud formation is more

286 sensitive to the under-cloud and near-surface water vapor content, similar to vertical

287 velocity, relative humidity (RH) data at 800 hPa (RH_{800}, for regions with TH

288 $\geqslant$ 1000 m), 900 hPa (RH_{900}, for regions with TH<1000 m) are employed and

289 the specific humidity at 2 m (q) is adopted to represent the

290 near-surface water vapor content.

291 ~~We obtained all these parameters at a spatial resolution of 0.5°×0.5°, and a temporal~~

292 ~~resolution of 3 hours. Based on the findings in previous studies,~~

3. Methods

3.1 A convective cloud identification method

Numerous previous studies have attempted to develop methods for detecting and classifying cloud features, including convective clouds, based on satellite observations. One of the most common methods for identifying cloud is thresholding (Williams and Houze Jr., 1987). However, Wielicki and Welch (1986) found that the identified cloud fraction depends strongly on threshold values, as cumulus cloud reflectance varies greatly within individual clouds and at cloud edges. As a result, many studies now adopt digital image processing to help identify shallow convective clouds more accurately.

One widely used image processing method is textural analysis, which adopts second-order statistics representing the texture of the digital image, as first proposed by Haralick (Haralick et al., 1973). This method, known as the gray level co-occurrence matrix (GLCM) method, was applied by Welch et al. (1988a);(1988b) in their LandSat data analysis of marine stratocumulus cloud texture. The GLCM is a matrix of counts/frequencies of grey values for pairs of pixels, whose relative positions are defined by the polar coordinates (d, θ). The formula can be written as:

$$GLCM(i,j,d,\theta) = Pr\{I(x_1,y_1) = i, I(x_2,y_2) = j\} \ x_1, x_2 \in m \ and \ y_1, y_2 \in n \quad (1)$$

where $Pr\{E\}$ denotes the probability of event E, I represents the image matrix of size m×n (in this study, m = 1251, and n = 1001, as both the zonal and meridional spatial resolutions are 0.02° in the ROI), (x_1,y_1) and (x_2, y_2) are the two elements in I with gray tone value i and j, which are separated by distance d in direction θ. The unit of d is a pixel, and θ always takes 0°, 45°, 90°, and 135°. The maximum difference between i and j defines the size of GLCM. When the frequency of the $(i, j)^{th}$ element is more concentrated near the off-diagonal of the GLCM, the image contains more complex texture (Figure S1). To define texture properties from the GLCM, several image statistical variables are derived from this matrix, including "contrast", "homogeneity",

319 "energy", and "entropy" , etc. (Haralick, 1979;Welch et al., 1988c;Baum et al.,
320 1997;Bottino and Ceballos, 2014). ~The "contrast" measures the intensity contrast
321 between a pixel and its neighbors, assessed over the entire image. "Homogeneity"
322 measures the closeness to the diagonal of the GLCM element distribution. "Energy",
323 also termed the angular second moment, measures the complexity of the image, and
324 "entropy" measures the degree of randomness.s, evaluated over the entire image. The
325 formulas are:

326 $Contrast = \sum_{i,j}|i-j|^2 GLCM(i,j)$ (3)

327

328   The objective of this section is to identify new and mature convective clouds.

329 $Energy = \sum_{i,j} GLCM(i,j)^2$ (5)

330 $Entropy = \sum_{i,j} GLCM(i,j)\ln[GLCM(i,j)]$ (6)

331 T The objective of this section is to identify new born and mature convective clouds.
332 As the edges of convective clouds tend to be very sharp (Purdom, 1976) in visible
333 channel images, large differences between i and j occur. Thus, can produce large
334 'contrast' values can be found (Equation 32) at the edge of convective clouds. The
335 formula is:

336 $Contrast = \sum_{i,j}|i-j|^2 GLCM(i,j)$ (2)

337   We use the mean "contrast" data at d=1 in the four directions
338 (θ=0°, 45°, 90°, and 135°) calculated from the visible channel (0.64 μm) to identify
339 convective clouds.

340   Besides this parameter, we also employ the visible reflectance (VIS, 0.64 μm) and
341 brightness temperatures (T_b) at 11.2 μm and 12.4 μm to help identify the distinctive
342 patterns of convective clouds. The spatial gradient of T_b (11.2 μm) helps exclude very

343 low-elevation fogs, whose temperatures are close to that of the surface in the morning.
344 We use these three parameters in a k-means clustering analysis. Five clusters are
345 classified, and the mean contrast values are calculated. Those clusters with relatively
346 higher "contrast" (with mean ~~Contrast~~contrast>3.5, which is the second smallest among
347 all the cluster mean contrast values) are considered either small convective clouds or
348 the edges of mature convective clouds.

349 Unlike stratus clouds produced by large-scale systems, mature local convective cloud
350 tops tend to have very high VIS reflectance and small area (Lima and Wilson, 2008).
351 As the cloud tops of mature convective clouds are also relatively flat, they produce
352 small "contrast" values. We consider those clusters having area smaller than 40,000
353 km^2 (10,000 pixels), mean VIS reflectance larger than 0.75, and maximum VIS
354 reflectance larger than 0.9 as the tops of mature convective clouds.

355 In addition, we adopt the split window technique to exclude cirrus (Mecikalski and
356 Bedka, 2006). The brightness temperature differences between 11.2 μm and 12.4 μm
357 are near-zero for convective clouds, and we exclude those pixels with brightness
358 temperature differences less than -4K. This allows us to produce a
359 cloud mask with a high probability of isolating convective clouds. Figure 2 shows the
360 entire flowchart of our convective-cloud identification method.

361 As we identify convective clouds using the combined results from texture analysis,
362 clustering, and thresholding, we name this cloud identification method the Texture-
363 Clustering-Thresholding-Convection IDentification (TCT-CID) method.

364 **3.2 Validation of the convective cloud mask**

365 Figure 3 presents t~~Two~~ examples of ~~the identified~~ convective clouds identified ~~mask~~
366 ~~from~~in the hilly regions in southern China at 13:40 LT on July 30th, 2016 and ~~from~~in
367 the mountain regions in northern China at 14:20 LT on June 22nd, 2016 ~~are shown in~~
368 ~~Figure 3~~. To get a general idea of the performance of ~~validate~~ the TCT-CID method, we
369 compare ~~the our~~the identified convective cloud masks ~~identified with our cloud mask~~

against the MODIS/Aqua MYD35 cloud mask. As the MODIS product does not classify clouds into different types, ~~we use~~ a scene which contains a vast convective cloud field and a scene with sparse convective clouds are chosen~~a scene from the hilly regions in southern China at 13:40 LT on July 30ᵗʰ, 2016 as an example. It contains a vast convective cloud field.~~, and most of the clouds in this scene are convective clouds.~~ Figure 3a and 3d shows the true-color image of the scene we chose. Figures 3b, e ~~and~~ 3c, f are the MODIS cloud mask data and the convective cloud mask from our method, respectively. We can see that there is a relatively good agreement between the MODIS cloud mask and that identified by our method, especially for the deep convective clouds.

The method is designed to find sharp edges and bright clusters in VIS images firstly, but as some of the high clouds may also fit these conditions, which are not the subject of this study, we added a split-window filter to exclude this kind of clouds. However, the addition of this filter will also exclude the anvils of some mature convective clouds and some of the shallow clouds, so the cloud area identified by our method is smaller than the cloudy area found by the MODIS cloud mask and the capability of shallow convection identification is limited. Nevertheless, the majority of convective clouds are well captured by our method.

In order to validate the result of convective clouds identified by the TCT-CID method statistically, we compared the identified convective cloud mask with the Himawari-8 Level 2 cloud type data from the L2CLP010 product (see https://www.eorc.jaxa.jp/ptree/userguide.html; last accessed: May 2020). This product provides the cloud type information using the ISCCP cloud classification criteria, which defines cloud type using specific combinations of cloud top pressure (CTP) and cloud optical thickness (COT) (Rossow and Schiffer, 1991). A COT-CTP diagram is created to differentiate cloud types with different radiative feedbacks.~~, so~~ ~~T~~this method provides to some degree an accurate ~~description~~identification and classification of various cloud types. In this study, we compared the identified convective cloud masks

with the L2CLP cloud type product. TThe frequencies of different cloud types corresponding to the identified convective cloud masks are calculated as the percentage of the convective cloud mask pixel count that matches each ISCCP cloud type to all the cloud mask pixelsshown in (Figure S1S2)-. We can find that the frequencies of DCC and Sc are relatively significant, especially around noon time, which indicates that the TCT-CID method is effective at identifying deep convective clouds and stratocumulus clouds. Other cloud types, such as altostratus, nimbostratus and cumulus cloud also show relatively large amounts. These cloud types can be seen as representing different stages in the development of convective clouds. Although their frequencies only exceed the median but not the 2σ values of the distributions, they still show significant differences from the frequency of cirrus, stratocirrus, altocumulus and stratus. After 16:00, as the solar zenith angle grows, the cloud top reflectance increases significantly. The criteria of the TCT-CID method become less strict, so that cloud identification errors increase. Nevertheless, the frequency of DCC still passes the 2σ line, which implies that deep convection is the most robust cloud type that can be identified by the TCT-CID method.

These results suggest that the identification by the TCT-CID method is relatively reliable in studying the convective cloud properties and their relationship with aerosols.

4. Results and discussion

4.1 The diurnal cycle of convective clouds

We use the L1 data from Himawari-8 acquired from May to September in 2016 and 2017 to identify local convective clouds over eastern China and build the spatial distribution of convective clouds. Figure 4 shows the frequency of convective clouds occurring between 08:00 and 17:00 LT, calculated by dividing the number of convective clouds observed in six observations per hour (one every 10 minutes, e.g. from 08:00-08:50) by the accumulation between 08:00 and 17:00aggregated over the entire study period. The study period isincludes 20455 Himawari images, containing more than

425 2000 samples within each pixel ~~within~~ each hour. Convective cloud occurs
426 predominantly over the sea in the morning, and gradually shifts inland after local noon.
427 This convective cloud occurrence pattern is driven by distinct differences in the specific
428 heat capacities and boundary-layer thermodynamics over land and ocean. In the
429 morning, radiative cooling and land-breeze contribute to the formation of convective
430 clouds over the ocean, whereas temperatures near the land surface tend to be relatively
431 low, which makes it difficult for convective clouds to form there at this time of the day.
432 But in the afternoon (local time), as land surface temperatures increase, the near-surface
433 air layer becomes more unstable, making it easier for convective clouds to form. The
434 accumulation of land-surface heating during the day also favors the development of
435 deep convection in the afternoon. Such patterns are highly consistent with previous
436 studies (Garreaud and Wallace, 1997;Sui et al., 1997;Yang and Slingo, 2001;Li et al.,
437 2010).

438 To further validate the identification results, the statistical patterns of convective
439 cloud masks are investigated in Figure 4 and 5. The impact of diurnal solar radiation
440 variation and topography on convective clouds are already well-understood (Houze Jr.,
441 2012;2014), and thus, these results serve as further support for our cloud identification
442 method. The black lines in Figure 4 mark the 1000 m surface elevation contour,
443 which is approximately the boundary between the plains and elevated terrains. Around
444 13:00-14:00 local time, convective clouds begin to form over the elevated regions, and
445 the amount begins to increase afterwards (Figure 4).

446 Figure 5 shows the joint distribution of convective cloud occurrence frequency (CC
447 OF) anomaly with respect to terrain height (TH) over land and associated
448 meteorological factors. Vertical velocities and relative humidity at 800 hPa and
449 900 hPa   are   used   as   proxies   for   the   basic   state   of   dynamics
450 and water vapor for regions with elevation above and below 1000 m, respectively.

451 Due to the different sample sizes over terrains of different ~~heights~~elevations (Figure

S3)~~Generally,~~ CC OF~~s~~ tend to ~~has~~ have two peaks, at heights below 500 m and above 1000 m (Figure 5a-d)~~, which is likely due to the different sample sizes over terrain of different heights (Figure S2)~~. Thus, the mean values and standard deviations are calculated below and above 1000 m, respectively. ~~Nevertheless, the thermal factors that impact convective cloud occurrence show strong differences between lower and higher elevation surfaces.~~ Convective clouds tend to require more unstable ~~thermal~~ conditions and higher surface potential temperature. The ~~over regions with higher surface elevation compared to regions with lower surface elevation (TH≤1000 m). The~~ LTS CAPE can be 0.0~~5~~2~0.19 kJ/~~10~~K ~~lower~~higher when convective clouds occur compared ~~with the~~ all-sky conditions, and the differences can be about 0.05~0.1kJ/K larger over higher terrains (TH>1000 m)~~,~~. ~~T~~whereas ~~t~~he mean value~~s~~s of ~~potential temperature θ~~ are always slightly ~~higher~~larger than under clear-sky conditions when convective clouds occur. Further, θ values ~~can be~~increased by nearly 10K ~~higher,~~ for convective clouds to be favored at higher elevations. ~~Further, instability and surface heating are also stronger when convective cloud occurrence is favored after about 11:00 LT relative to the early morning.~~ For dynamical conditions, shown in Figure 5i-p, compared with the all-sky conditions, the ~~mean values of~~ CC OF for both $\omega_{850-800}$ and $\omega_{925-900}$ tend to move slightly in the negative direction ~~are negative~~ (i.e., upward motion) ~~and tend to move slightly in the negative direction a~~and become stronger from 08:00 to 14:00, with about 0.042 Pa/s and 0.018 Pa/s ~~dropping~~decreases in the mean values for the higher and lower terrains, respectively~~, acting as a nonnegligible contributor to the diurnal variation of convective clouds during the day.~~ The differences are always larger over higher altitude regions especially around 14:00 LT.

The under-cloud relative humidity (RH) values (~~RH_{700}-~~RH_{800} and ~~RH_{850}-~~RH_{900} for regions of TH>1000 m and TH≤1000 m, respectively) show a general increase ~~from 08:00 to 14:00~~ when convective cloud~~s~~ occur, ~~and whichand~~ are close~~r~~ to 100% compared ~~with theto~~ all-sky conditions ~~when cloud occurrence is most common~~. In addition, the under-cloud RH over lower terrain is always higher than it is over higher-

altitude regions during daytime (Figure 5q-x). ~~This pattern may also be caused contributed by the~~The stronger surface heating over higher terrain, which decreases the RH, may also contribute to this pattern ~~near the surface~~. Also note that where convective clouds occur, specific humidity ~~at~~near the surface (q) is always higher. ~~And~~ T~~t~~he mean q values are always about 4~6g/kg larger for regions having TH≤1000 m than for regions where TH>1000 m (Figure 5y-z2). This might indicate that, compared with higher terrain regions, it is always moister over lower terrain, so it is more difficult for cloud droplets to evaporate in such places. ~~q over regions with TH>1000 m decreases more rapidly than for lower altitude regions from 11:00 to 17:00, but RH$_{700}$ increases at higher altitudes, probably indicating that moisture over higher terrain is transported to higher altitudes to form convective clouds at these times.~~

All these thermal, dynamical and moisture conditions show relatively significant differences between the convective-cloud conditions and the all-sky conditions, which indicates that the formation and development of convective clouds favor strong instability, surface heating, vertical velocity and water vapor supply. Such patterns show that our data conform to the expected patterns and can be used for Such patterns show that our data conform to the expected patterns and can be used for the analysis presented below.

4.2 Changes in convective cloud diurnal cycle associated with aerosol

In this study, PM$_{2.5}$ observations from 1205 stations over eastern China are used as proxies for CCN, to roughly separate clouds into polluted and clean classes. We match the hourly measured PM$_{2.5}$ with the 10 min convective cloud identification results by supposing the convective cloud observed in the same hour occurs under the same PM$_{2.5}$ conditions. For each site, we use the top quarter of the PM$_{2.5}$ concentration distribution as the criterion for identifying polluted cases, and the bottom quarter as the clean cases (Figure 6). We then aggregate them into a 0.4°×0.4° grid using nearest neighbor interpolation to create clean and polluted ~~threshold~~ fields. The average clean and

polluted thresholds over the ROI are shown as dashed and solid red lines in Figure 6. All the convective clouds with their centroids located in the grid box are classified using the clean and polluted threshold value for that grid box. ~~Only those clouds with centroids~~ The centroids of convective clouds located within a grid box having $PM_{2.5}$ concentration greater (less) than the polluted (clean) threshold are deemed as polluted (clean) convective clouds ~~located within a grid box classified as polluted (clean) are deemed as polluted (clean) convective clouds~~. We calculated the convective cloud fraction (CCF) using the number of convective clouds under polluted (or clean) conditions divided by the total convective cloud amount within each grid cell. On average, 4.6×10^7 (4.1×10^7) pixels are deemed as clean (polluted) convective cloud within each hour. Figure 7 shows the difference of CCF in polluted and clean environments. Warm (cold) colors in the figure mean that there are more (less) convective clouds under the polluted condition. Additionally, only those data points that exceed the 95% significance level according to the Pearson's χ^2 test are plotted. From Figure 7a to 7e, we find that before 12:00 LT, convective clouds under polluted conditions generally occur in larger amounts, especially over the plateau region and some of the mountain regions. This pattern reverses gradually from 13:00 to 17:00 LT (Figure 7f-7j): the amount of convective clouds under polluted conditions tends to diminish, relative to those in clean conditions, in the afternoon. However, in several places, the CCF difference generally persists from morning to afternoon. Some red dots in southern and eastern China seem to occur over megacities, presumably ~~caused by~~ related to the co-action of high aerosol loading and the urban heat island effect (e.g., for the megacities around Yangtze River Delta (YRD) and the Pearl River Delta (PRD), marked by black circles in the figure). There are also red dots located near several mountain areas, as complex topography may also ~~also~~ be related to such a phenomenon. Furthermore, different topography may also lead to different convective cloud response to aerosol loading. Over northern China, more convective clouds form over mountains under polluted conditions, whereas over the central China plain, with mountains around,

536 convective clouds may be suppressed all the time by high aerosol loading. The number
537 distribution of convective cloud clusters in each area bin, aggregated over the entire
538 ROI is shown in Figure ~~S3~~S4. Polluted convective cloud covers a larger area than clean
539 convective cloud early in the day; this pattern gradually reverses after 13:00 LT, starting
540 from the decrease in number of smaller convective cloud clusters. And after 14:00 LT,
541 convective cloud area under clean conditions dominates. This pattern may suggest that
542 high aerosol loading is perhaps~~probably~~ one of the factors that inhibit~~sing~~ the formation
543 of small convective clouds ~~via the aerosol radiative effect~~ in the afternoon.

544   In an attempt to assess the effects of pollution on diurnal convective cloud behavior,
545 the influence of other meteorological factors is addressed later in section 4.4 by
546 stratifying the data based on such factors. We note here only that a relatively clear
547 diurnal pattern in CCF exists, and that pollution effects appear to be correlated with this
548 pattern.

549   Koren et al. (2008) demonstrated two opposite effects of absorbing aerosol on cloud
550 cover, i.e. the microphysical effect and the radiation effect, by theoretical derivation,
551 and verified this theory with observations in the Amazon region. Their study concluded
552 that aerosol particles can increase cloud droplet number by serving as CCN. However,
553 when aerosol concentration is higher, the attenuation of solar radiation by aerosol
554 particles decreases the surface temperature, and atmospheric heating decreases the lapse
555 rate, thus ~~inhibits~~inhibiting sensible heat flux(Feingold et al., 2005). The decrease in
556 the surface temperature also reduces evaporation ~~moisture flux, thus suppressing~~
557 ~~convection~~(Koren et al., 2004), so that the atmosphere becomes drier and more stable,
558 which ~~will~~ suppress convection. As aerosol loading increases, surface temperature tends
559 to decrease regardless of aerosol type (Gu et al., 2006;Jiang et al., 2013;Yang et al.,
560 2016a;Yang et al., 2016b;Yang et al., 2018). Thus, we can infer that under conditions
561 of high aerosol loading, the vertical moisture flux may be suppressed, which would
562 inhibit convective cloud formation. Therefore, investigating the diurnal variation of
563 aerosol microphysical and radiative effects might help explain the patterns shown in

564   Figure 7.

565   Figure 8 shows the relationship between convective cloud and $PM_{2.5}$ concentration.
566   Ten equally sampled bins of $PM_{2.5}$ concentration were defined, and we calculated the
567   mean CCF within each bin using the convective cloud amount in each $PM_{2.5}$ bin divided
568   by the total convective cloud amount within the same area for all $PM_{2.5}$ values. Sample
569   sizes are shown in the color shaded background in each subfigure, and the mean sample
570   number within each $PM_{2.5}$ bin is ~ 8×10^5. The three-point moving average of the values
571   is also plotted. We find that CCF first increases with respect to $PM_{2.5}$ mass concentration
572   and then starts to decrease; this pattern persists throughout the day. The $PM_{2.5}$ mass
573   concentrations at all turning points of the curves are between 20 μg/m^3 and 30 μg/m^3.
574   Similar results were also found by previous studies (Guo et al., 2017;Jiang et al.,
575   2018;Wang et al., 2018). Adding to these previous results, we find that the relationship
576   of $PM_{2.5}$ and CCF persists throughout the day, as we have used high-resolution
577   geostationary satellite data that provide us ample samples at different times.
578   Furthermore, the aerosol effect on convective cloud is likely to be robust not
579   only for deep convective clouds, but also for convective clouds at any stage of
580   development. This pattern might be attributed to the competition between the
581   microphysical effect dominating at low $PM_{2.5}$ concentration, and the radiative effect
582   becoming increasingly important at higher $PM_{2.5}$ concentration. This may also explain
583   the phenomenon in Figure S4. As solar radiation begins to wane in the afternoon,
584   surface heating weakens, the high aerosol loading would suppress
585   convection via the dominance of radiative effect, thus inhibit the formation of small
586   convective clouds.

587   The CCF values corresponding to the average thresholds identifying clean and
588   polluted conditions (marked as vertical red dashed line pairs with numbers in each
589   Figure 8 panel) generally tend to be higher under polluted than under clean conditions
590   from 08:00-11:00 LT, whereas from 12:00-17:00 LT the pattern gradually reverses. The

591 shapes of the moving average curves change slightly from morning to afternoon

592 compared with the mean CCF over all times (~~magenta~~ red dots), where CCF is lower

593 in the morning before the tipping point but higher in the afternoon, and after the tipping

594 point, CCF is higher in the morning but lower in the afternoon. As we found from

595 Figures 5 and 7, meteorological condition changes associated with topography and

596 diurnal solar radiation variations may play roles in altering the shapes of the CCF curves.

597 For conditions with PM$_{2.5}$ concentrations lower than the 20~30 μg/m^3 turning zone,

598 more convective cloud is formed, ~~probably~~ presumably due to more unstable

599 environments and stronger surface heating, especially in the afternoon. But as both the

600 surface and the air above ~~is~~ are generally moister before noon time (Figure ~~5x~~5q-z2)~~,~~

601 ~~especially at higher terrains~~, the higher ~~q~~moisture may suppress cloud droplet

602 evaporation and thus keep CCF from sharply decreasing.

4.3 Effects of topography on the aerosol-convective-cloud relationship

604 In order to isolate the potential effect of topography on the aerosol-

605 convective-cloud relationship, we further investigate in this section the CCF changes

606 along with TH at different levels of aerosol loading. The CCFs at different TH in

607 both polluted and clean conditions are shown in Figure 9. The CCF under clean (or

608 polluted) conditions within each elevation bin h is calculated using the formula shown

609 below:

$$CCF_{C(P)}(h,t) = average\left(\frac{N_{C(P)}|_h(i,j,t)}{N_{total}|_h(i,j)}\right) \times 100\% \tag{3}$$

611 where N$_{C(P)}$|$_h$(i,j,~~h,~~t) represents the number of convective clouds occurring under clean

612 (C) or polluted (P) conditions in the (i,j)th pixel box in the ROI ~~in elevation bin h~~ during

613 hour t, and N$_{total}$|$_h$(i,j,~~h~~) represents the total number of convective clouds observed in

614 each pixel box ~~at elevation bin h~~ during the ~~daytime~~08:00-17:00 daytime period. For

615 each CCF bin in Figure 9, i and j ~~locates~~denote the pixels within the region having

616 elevation h. ~~–~~Sample sizes are shown in Figure ~~S2~~S3. We find that the CCF difference

617 between polluted and clean conditions generally agrees with Figure 7 in that CCF is

618 higher for polluted cases in the morning, lower in the afternoon, and the differences are
619 statistically greatest in early morning and late afternoon. In addition, the CCF
620 differences between polluted and clean conditions vary considerably along with
621 increasing TH, which may indicate that the effects of topography and air quality on
622 CCF co-vary, and the impact of topography might be much stronger compared with
623 increased aerosol loading.

624   There is also another aspect of these phenomena. In Figure 10, by normalizing the
625 occurrence frequencies by the total number of polluted and clean cases within each hour,
626 respectively, we explore how topography changes the polluted and clean convective
627 clouds   spatially.   The   normalized   CCF   (NCCF)   is
628 computed as:

629
$$NCCF_{C(P)}(h,t) = average\left(\frac{N_{C(P)}|_h(i,j,t)}{\sum_m \sum_n N_{C(P)}(m,n,t)}\right) \times 100\%$$

630   (4).

631 The mean NCCF is also calculated with i and j withinat each elevation bin h. Unlike
632 CCF (Equation 73), the denominator for NCCF (Equation 84) is not summed over all
633 studied times-of-day but over the entire ROI (the size of which is m×n pixels) within
634 each hour. because Because the elevation-related response reverses over the day (e.g.,
635 Figure 9), NCCF focuses more specifically on how CCF at a given location and terrain
636 elevation compares with all locations at the same elevation and the same time, reducing
637 the influence of diurnal variation and emphasizing elevation-related differences. As
638 such, the difference in NCCF between clean and polluted cases reflects the difference
639 caused by topography when the overall environment is under clean or polluted
640 conditions. We can see from Figure 10 that below the elevation of 500 m, most of the
641 convective clouds are suppressed under polluted conditions, whereas over regions with
642 terrain height greater than 1000 m, the amount of convective cloud under polluted
643 conditions is significantly larger, especially before 14:00 LT. This phenomenon may
644 partly explain the results shown in Figure 7, where complex topography plays an

645   important role in the aerosol effect on convective clouds. Under polluted conditions,

646   convective clouds over lower terrain are much easier to suppress, whereas over elevated

647   terrain, convective clouds are more likely to be invigorated.

648   As the topography over eastern China has a general step-like distribution, we

649   roughly separate the terrain heights into four bins representing the plains (0-500 m),

650   mountain ranges (500-1000 m), plateau (1000-1500 m) and high mountains (1500-2000

651   m), and assess how the aerosol effect changes over different topography. The pixel

652   number within each bin is over $4.0\times10^5, 1.6\times10^5, 2.3\times10^5$ and 0.5×10^5. We calculate

653   the CCF ~~within each of the 10 equally sampled PM$_{2.5}$ bins over each sub-region~~using

654   the number of convective clouds within each of 10 equally sampled PM$_{2.5}$ bins divided

655   by the total convective cloud amount over each sub-region. Each pair of CCFs in the

656   four sub-regions is significantly different at 95% significance level according to the

657   Student's t-test. Figure 11 shows how cloud fraction changes with respect to PM$_{2.5}$

658   concentration over the four different terrain elevation ranges. In all four sub-regions,

659   CCF first increases with PM$_{2.5}$ concentration and then decreases. But before the turning

660   zone (between 20~30 μg/m^3) the CCF is slightly higher over mountains and plateaus

661   than over the plains, but after the turning zone, this pattern generally reverses. This

662   ~~probably~~ presumably occurs because instability and surface heating are stronger over

663   the higher terrain, which invigorates the convective cloud development by enhancing

664   the aerosol microphysical effect (Rosenfeld and ~~Ulrike~~ Lohmann, 2008). The air over

665   the plain regions is moister than that over the mountain and plateau regions, which

666   suppresses droplet evaporation thus tends to overtake the aerosol radiative effect. ~~that~~

667   Over higher terrains (TH>1000m), aerosol concentrations are relatively low, and the

668   effect of topography might play a more important role. Surface heating is relatively

669   stronger at the high mountains (TH>1500m), which may dominate the trend of

670   decreasing CCF after the turning zone, so that the inhibition of convective cloud by

671   aerosol radiative effect is weaker, and the CCF is higher than the plateau regions

672   (1000<TH≤1500m) after the turning zone.

673   In order to further investigate the ~~probable~~potential effect of topography in aerosol-

674   convective-cloud relationship, the vertical circulation and moisture distributions are

675   studied. We have classified ~~each~~the reanalysis data ~~grid cell~~ into clean and polluted

676   cases using the clean and polluted threshold fields described in section 4.2. The

677   meridional-vertical mean distribution of relative humidity and wind are then calculated

678   (Figure 12). ~~The meridional-vertical distribution of relative humidity and wind are~~

679   ~~shown in Figure 12.~~ Generally, the circulation pattern is consistent throughout the day~~;~~

680   the updraft south to 35°N is always stronger than that over the northern region, and the

681   relative humidity in this region is significantly higher. Under clean conditions, the

682   strong updraft and southerly wind south to 30°N may bring large amounts of moisture

683   inland, contributing to convection development in this region. But under polluted

684   conditions, the southerly wind is weaker, and the relative humidity above this region is

685   lower, which may ~~lead to~~provide a restraint ~~of~~ on convective cloud development ~~due to~~

686   ~~the inhibition of aerosol microphysical effect~~. Both the drier conditions and the

687   increased ~~in~~ aerosol loading ~~are~~ likely ~~to~~ contribute to the inhibition of convective cloud.

688   In regions north to 35°N, there is an obvious north wind component under clean

689   conditions, bringing dry and clean air to this region, which may suppress the

690   development of convective clouds. But under polluted conditions, under the control of

691   a relatively strong southerly wind, moisture and pollutants may be blown toward the

692   mountain regions and be forced upward ~~to be uplifted~~ by the elevated terrain,

693   strengthening the formation and development of convective clouds, especially over the

694   windward slopes north to 40°N. The zonal-vertical wind and relative humidity changes

695   are shown in Figure ~~S4~~ S5 and ~~S5~~S6. The updraft along windward slopes is always

696   stronger, especially under polluted conditions in the northern part of the ROI. This is

697   likely to contribute to strengthening the aerosol microphysical effect over such regions,

698   which facilitates the invigoration of convective clouds. All the patterns described above

699   agree well with the phenomena identified in the previous figures, indicating that

700   different circulation patterns and the changes associated with different topography may

701 have a considerable impact on the variability of the aerosol-convective-cloud
702 relationship.

4.4 The environmental dependence of the aerosol effect

704   To further isolate the signal of aerosol effects from that of meteorological conditions,
705 and to characterize the co-variation of topography and aerosol effects on convective
706 clouds, the changes of CCF with aerosol loading under various thermodynamic,
707 dynamical and humidity conditions at different time-of-day and over different terrain
708 heights are shown in Figures 13 and 14. Note that vertical velocities (relative
709 humidity) at 800 hPa and 900 hPa are used to
710 represent the basic dynamics (water vapor) state for regions with elevation above and
711 below 1000 m, respectively. We defined ten equally sampled bins of $PM_{2.5}$
712 concentration and calculated the joint distribution of CCF along with each $PM_{2.5}$ and
713 meteorological factor bin, the sample sizes in each subfigure are shown in Table S1
714 and S2. Generally, the CCF along with $PM_{2.5}$ concentration shows unimodal
715 distributions, CCFs increase at first and then decrease with $PM_{2.5}$ concentration, as we
716 saw in Figure 8, but now within each of the vertical velocity and relative humidity strata,
717 i.e., where we have minimized the differences in meteorological conditions.
718 The patterns are consistent at different time-of-day and over different topography,
719 which may indicate that under different thermodynamic, dynamical and water vapor
720 conditions the competition between the aerosol microphysical and radiation effects
721 always exists, no matter how meteorological conditions vary, at least within the study
722 domain. The main difference in the $PM_{2.5}$-CCF relationship under different
723 meteorological conditions lies in the tipping point.

724   The mean tipping point of CCF curves at different values of meteorological variables
725 is marked as the turning line between the increasing and decreasing CCF trends (red
726 dashed lines in Figures 13 and 14). From Figure 13a-h, the turning line moves to smaller
727 $PM_{2.5}$ values as surface heating increases and the atmosphere becomes more unstable
728 from morning to late afternoon. The peaks of CCF move from stable (weak surface

設置了格式: 下标

heating) conditions to unstable (strong surface heating) conditions during the day (Figure 13a-h and 14a-h).And as CAPE (surface heating) isgets stronger in the afternoon and over lower terrains, the tipping point is smalleralso decreases (Figure 13a-h and 14a-h). This phenomenon may proveperhaps indicates that that changes in thermodynamic conditions attributed to diurnal solar radiation variation and topography are perhapsrobably among the potential impact factors that influence the changing CCF curve shapes in Figures 8 and 11. Stronger surface heating and more unstable conditions may increase CCF when the microphysical effect of aerosol dominates the CCF changes, and would potentiallyprobably strengthen the aerosol microphysical effect as smaller aerosol concentrations may induce the same extent of invigoration..

Updraft changes, which can represent under-cloud dynamical conditions, at 800 hPa and 900 hPa for terrain higher and lower than 1000 m, respectively, are relatively small during the day and over different topography. However, the turning values of CCF generally decrease with increasing updraft conditions as well (Figure 13i-p). This pattern is likely to indicate that more aerosol particles can be activated or entrained into the clouds from the boundary layer when uplift is stronger, which in turn might strengthen the aerosol microphysical effect. Further, as shown in Figure 14k-l, stronger updrafts over higher mountains (with TH>1500 m) invigorate convective clouds after the turning line, especially for $PM_{2.5}$ concentrations higher than 50 $\mu g/m^3$, which suggests that the suppression of convective clouds by aerosol radiative effect is counteracted.

For water vapor conditions, both higher relative humidity below cloud base (Figures 13q-x and 14q-x) and higher specific humidity at the surface (Figures 13y-z2 and 14y-z2) generally produce larger CCF. Higher RH and higher q are also associated with higher CCF peaks. These patterns are consistent with the previous studies (Koren et al., 2010), and may indicate that moister conditions can lead to greater activation of aerosol particles-. As $PM_{2.5}$ measurements are dried particle masses, which can minimize the

influences of ~~by the environmental~~ambient moisture, these patterns are more likely ~~to~~
~~be~~ related to~~indicate that moister conditions can lead to greater activation of aerosol~~
~~particles, which may~~ the strengthen~~ing~~~~en~~ the ~~of the~~ aerosol microphysical effect,~~ and~~
which might overtake the suppression from the aerosol radiative effect in higher aerosol
loading conditions in these regions.

The meteorological factors that influence the aerosol effect on convective clouds are very likely to interact with one another, which may produce combined impacts on convective clouds and lead to nonlinear changes to the CCF distribution, creating large variations in the results. By analyzing the potential co-variation of aerosol effects, meteorological factors and the impact of topography on convective clouds, we find that the CCF changes are robust under a range of meteorological conditions, as the strength of both the aerosol microphysical and radiative effects can potentially be influenced by specific thermodynamic, dynamical and humidity conditions.

However, identifying the apparent correlations between convective cloud and aerosol loading is only a first step, supporting the hypothesized mechanisms by which aerosol affects convective cloud occurrence. The mechanism by which the aerosol and meteorology interact is another important question, that is beyond the scope of the current study. If synoptic factors, differences in meteorological conditions associated with topography and aerosols work together, determining which factors dominate the formation and development of convective clouds needs to be explored with deeper mining of the data, as well as modeling studies, in the future.

5. Summary

Following rapid economic development and industrialization, eastern China has

783 faced increasingly severe air pollution during recent decades. Aerosols, which play an
784 important role in the formation and development of clouds and precipitation, can be
785 among the main factors influencing urban inundation, hail and severe storms.

786   The interaction between aerosol, weather, and topography is complex, so untangling
787 their effects, that jointly influence convective cloud formation, is difficult. This study
788 applies very large, diurnally resolved geostationary satellite data and extensive ground-
789 based observations to investigate the characteristics of convective clouds, the impacts
790 of aerosol on convective cloud properties, and the potential mechanisms that define the
791 aerosol impacts on convective clouds under different meteorological conditions and
792 over different topography. Having such large data sets allows us to stratify by various
793 factors and isolate patterns among the multiple dimensions. The key results of this study
794 are as follows:

795   •   We develop a convective cloud identification process named the TCT-CID
796   algorithm by combining the merits of texture analysis, a clustering technique, and
797   a threshold method, using the Level 1 data from the Japanese geostationary satellite
798   Himawari-8 during the period from May to September in 2016 and 2017. The
799   method offers stable and relatively accurate performance in identifying convective
800   clouds.

801   •   The cloud mask is used to study the occurrence frequency and the regional
802   distribution of convective clouds over eastern China, first to determine whether the
803   new data reproduce expected cloud-occurrence patterns. Statistical results show
804   that convective cloud occurrence frequency (CC OF) is higher under more unstable
805   conditions with stronger surface heating and updraft. And in the afternoon, this
806   phenomenon is more significant than in the morning. The increases in both under-
807   cloud relative humidity and surface specific humidity produce higher CC OF
808   during the day. There is also a significant difference between higher and lower
809   terrain regions. The consistency of these patterns with previous studies and the

classic theories of convective cloud formation helps validate the results of the TCT-CID algorithm.

- We then compared convective clouds under clean and polluted conditions, and further examined the possible impact of the diurnal cycle and topography on the aerosol-convective-cloud relationship. We find that the convective cloud fraction generally tends to be larger before noon and smaller in the afternoon under more polluted conditions, but megacities and complex topography can influence the pattern. This result provides a new perspective on the aerosol effect compared to previous studies.

- A relationship between aerosol loading and convective cloud fraction is found. The cloud fraction increases initially, but then decreases with successive increases in aerosol loading. This pattern is consistent with the combined action of the aerosol microphysical and radiative effects. Previous studies found similar results for deep convective cloud and convective precipitation studies, but by using high-resolution geostationary satellite observations, we further find that this pattern is probably robust for convective clouds at all stages of development.

- A possible alternative explanation is that aerosols and CCF are associated because they are both affected simultaneously by the same meteorological factors. However, CCF had generally similar relationships with aerosol mass concentrations for all meteorological stratifications that were examined. This observation renders the alternative meteorological explanation less likely.

- Although the aerosol-convective-cloud relationship is relatively stable, some variability also exists. The pattern varies throughout the day depending on terrain height, and is modulated by varying thermodynamic, dynamical and humidity conditions during the day. More unstable environment and stronger surface heating would invigorate the convective cloud development, whereas moister conditions might suppress droplet evaporation thus tends to overtake the inhibition of

837   convective clouds.

838 • We find that the meteorological variations driven by diurnal solar radiation changes

839   and topography are among the potential reasons for changes in the

840   relationship between convective cloud and aerosol loading, which could be related

841   to the changes in the relative strength of aerosol microphysical and radiative effects.

842   Over higher terrains such as mountains and plateaus, a southerly wind component

843   is likely to contribute to the strengthening of the microphysical effect through

844   forced uplifting of pollutant and moisture, which invigorates convective cloud over

845   the windward slopes, whereas over plains areas, aerosol pollution blocking solar

846   radiation is likely to dominate, thus decreasing the surface heating and suppressing

847   convection by enhancing the radiative effect. However, as aerosol concentration,

848   synoptic meteorological factors and topography might work together in influencing

849   the formation and development of convective clouds, the phenomena found above

850   can also be affected by nonlinear interactions among these factors.

851 Moreover, the analysis of this study is based mainly on satellite observations, which

852 in themselves provide limited insight into the mechanism underlying the observed

853 patterns. In the current study, we aimed only at isolating the possible effects of

854 aerosol on convective cloud properties under different meteorological conditions.

855 However, further exploration, including model simulations and/or targeted in-situ or

856 aircraft observations, are still needed to reveal the specific mechanisms behind these

857 phenomena.

858

859 **Acknowledgment**

860 We acknowledge the JAXA P-tree system (http://www.eorc.jaxa.jp/ptree/) for

861 providing the Himawari-8 Level 1 data, and the Global Modeling and Assimilation

862 Office (GMAO) (https://gmao.gsfc.nasa.gov/reanalysis/MERRA-2/), for providing

863 MERRA-2 reanalysis data. We would also like to extend our sincerest thanks and

864 appreciation to the China National Environmental Monitoring Center for providing the

865 hourly $PM_{2.5}$ data. This study is supported by the Natural Science Foundation of China

866 (42030606, 41925022, 91837204), the Ministry of Science and Technology of China

867 National Key R&D Program on Monitoring, Early Warning and Prevention of Major

868 Natural Disasters (017YFC1501702, 2017YFC1501403). We would also like to thank

869 the anonymous reviewers for their thoughtful suggestions and comments.

870

设置了格式: 字体: (默认) Times New Roman, 12 磅, 字体颜色: 黑色

References

871

872 Ackerman, A. S., Toon, O. B., Stevens, D. E., Heymsfield, A. J., Ramanathan, V., and Welton, E. J.:
873   Reduction of Tropical Cloudiness by Soot, Science, 288, 1042-1047,
874   10.1126/science.288.5468.1042, 2000.

875 Albrecht, B. A.: Aerosols, cloud microphysics, and fractional cloudiness, Science, 245, 1227,
876   10.1126/science.245.4923.1227, 1989.

877 Altaratz, O., Koren, I., Remer, L., and Hirsch, E.: Review: Cloud invigoration by aerosols—Coupling
878   between microphysics and dynamics, Atmospheric Research, 140, 38-60,
879   10.1016/j.atmosres.2014.01.009, 2014.

880 Andreae, M. O., Rosenfeld, D., Artaxo, P., Costa, A. A., Frank, G. P., Longo, K. M., and Silva-Dias, M.
881   A. F.: Smoking rain clouds over the Amazon, Science, 303, 1337-1342, 10.1126/science.1092779,
882   2004.

883 Andreae, M. O.: Correlation between cloud condensation nuclei concentration and aerosol optical
884   thickness in remote and polluted regions, Atmospheric Chemistry and Physics, 9, 543-556,
885   10.5194/acpd-8-11293-2008, 2009.

886 Baum, B. A., Tovinkere, V., Titlow, J., and Welch, R. M.: Automated Cloud Classification of Global
887   AVHRR Data Using a Fuzzy Logic Approach, Journal of Applied Meteorology, 36, 1519-1540,
888   10.1175/1520-0450(1997)036<1519:accoga>2.0.co;2, 1997.

889 Bessho, K., Date, K., Hayashi, M., Ikeda, A., Imai, T., Inoue, H., Kumagai, Y., Miyakawa, T., Murata,
890   H., Ohno, T., Okuyama, A., Oyama, R., Sasaki, Y., Shimazu, Y., Shimoji, K., Sumida, Y., Suzuki,
891   M., Taniguchi, H., Tsuchiyama, H., Uesawa, D., Yokota, H., and Yoshida, R.: An Introduction to
892   Himawari-8/9— Japan’s New-Generation Geostationary Meteorological Satellites,
893   Journal of the Meteorological Society of Japan. Ser. II, 94, 151-183, 10.2151/jmsj.2016-009, 2016.

894 Bottino, M. J., and Ceballos, J. C.: Daytime cloud classification over South American region using
895   multispectral GOES-8 imagery, International Journal of Remote Sensing, 36, 1-19,
896   10.1080/01431161.2014.978953, 2014.

897 Boucher, O., and Quaas, J.: Water vapour affects both rain and aerosol optical depth, Nature Geoscience,
898   6, 4-5, 10.1038/ngeo1692, 2012.

899 Chakraborty, S., Fu, R., Wright, J. S., and Massie, S. T.: Relationships between convective structure and
900   transport of aerosols to the upper troposphere deduced from satellite observations, Journal of
901   Geophysical Research: Atmospheres, 120, 6515-6536, 10.1002/2015jd023528, 2015.

902 Chakraborty, S., Fu, R., Massie, S. T., and Stephens, G.: Relative influence of meteorological conditions
903   and aerosols on the lifetime of mesoscale convective systems, Proceedings of the National Academy
904   of Sciences, 113, 7426-7431, www.pnas.org/cgi/doi/10.1073/pnas.1601935113, 2016.

905 Chakraborty, S., Schiro, K. A., Fu, R., and Neelin, J. D.: On the role of aerosols, humidity, and vertical
906   wind shear in the transition of shallow-to-deep convection at the Green Ocean Amazon 2014/5 site,
907   Atmospheric Chemistry and Physics, 18, 11135-11148, 10.5194/acp-18-11135-2018, 2018.

908 Chang, A. T. C., Chiu, L. S., and Yang, G.: Diurnal Cycle of Oceanic Precipitation from SSM/I Data,
909   Monthly Weather Review, 123, 3371-3380, 10.1175/1520-0493(1995)123<3371:dcoopf>2.0.co;2,
910   1995.

911 Charlson, R. J., Schwartz, S. E., Hales, J. M., Cess, KLEY, J. A., Hansen, J. E., and Hofmann, D. J.:

域代码已更改

Climate Forcing by Anthropogenic Aerosols, Science, 255, 423-430, 10.1126/science.255.5043.423, 1992.

Chen, T. M., Guo, J. P., Li, Z. Q., Zhao, C. F., Liu, H., Cribb, M., Wang, F., and He, J.: A CloudSat Perspective on the Cloud Climatology and Its Association with Aerosol Perturbations in the Vertical over Eastern China, Journal of the Atmospheric Sciences, 73, 3599-3616, 10.1175/jas-d-15-0309.1, 2016.

Fan, J., Leung, L. R., Rosenfeld, D., Chen, Q., Li, Z., Zhang, J., and Yan, H.: Microphysical effects determine macrophysical response for aerosol impacts on deep convective clouds, Proceedings of the National Academy of Sciences, 110, E4581-E4590, 10.1073/pnas.1316830110, 2013.

Fan, J., Rosenfeld, D., Yang, Y., Zhao, C., Leung, L. R., and Li, Z.: Substantial contribution of anthropogenic air pollution to catastrophic floods in Southwest China, Geophysical Research Letters, 42, 6066-6075, 10.1002/2015gl064479, 2015.

Feingold, G., Eberhard, W. L., Veron, D. E., and Previdi, M.: First measurements of the Twomey indirect effect using ground-based remote sensors, Geophysical Research Letters, 30, doi:10.1029/2002GL016633, 2003.

Feingold, G., Jiang, H. L., and Harrington, J. Y.: On smoke suppression of clouds in Amazonia, Geophysical Research Letters, 32, L02804, 10.1029/2004gl021369, 2005.

Garreaud, R., and Wallace, J. M.: The Diurnal March of Convective Cloudiness over the Americas, Monthly Weather Review, 125, 3157-3171, 10.1175/1520-0493(1997)125<3157:tdmocc>2.0.co;2, 1997.

Garrett, T. J., Zhao, C., Dong, X., Mace, G. G., and Hobbs, P. V.: Effects of varying aerosol regimes on low-level Arctic stratus, Geophysical Research Letters, 31, L17105, 10.1029/2004gl019928, 2004.

Garrett, T. J., and Zhao, C.: Increased Arctic cloud longwave emissivity associated with pollution from mid-latitudes, Nature, 440, 787-789, 10.1038/nature04636, 2006.

Gelaro, R., McCarty, W., Suárez, M. J., Todling, R., Molod, A., Takacs, L., Randles, C. A., Darmenov, A., Bosilovich, M. G., Reichle, R., Wargan, K., Coy, L., Cullather, R., Draper, C., Akella, S., Buchard, V., Conaty, A., Silva, A. M. d., Gu, W., Kim, G.-K., Koster, R., Lucchesi, R., Merkova, D., Nielsen, J. E., Partyka, G., Pawson, S., Putman, W., Rienecker, M., Schubert, S. D., Sienkiewicz, M., and Zhao, B.: The Modern-Era Retrospective Analysis for Research and Applications, Version 2 (MERRA-2), Journal of Climate, 30, 5419-5454, 10.1175/jcli-d-16-0758.1, 2017.

Givati, A., and Rosenfeld, D.: Quantifying Precipitation Suppression Due to Air Pollution, Journal of Applied Meteorology, 43, 1038-1056, 10.1175/1520-0450(2004)043<1038:qpsdta>2.0.co;2, 2004.

Gryspeerdt, E., and Stier, P.: Regime-based analysis of aerosol-cloud interactions, Geophysical Research Letters, 39, L21802, 10.1029/2012gl053221, 2012.

Gryspeerdt, E., Stier, P., and Partridge, D. G.: Satellite observations of cloud regime development: the role of aerosol processes, Atmospheric Chemistry and Physics, 14, 1141-1158, 10.5194/acp-14-1141-2014, 2014.

Gu, Y., Liou, K. N., Xue, Y., Mechoso, C. R., Li, W., and Luo, Y.: Climatic effects of different aerosol types in China simulated by the UCLA general circulation model, Journal of Geophysical Research: Atmospheres, 111, 10.1029/2005jd006312, 2006.

Guo, J., Zhang, X., Wu, Y.-r., Zhaxi, Y., Che, H., La, B., Wang, W., and Li, X.: Spatio-temporal variation trends of satellite-based aerosol optical depth in China during 1980–2008, Atmospheric Environment, 45, 6802-6811, 10.1016/j.atmosenv.2011.03.068, 2011.

955 Guo, J., Deng, M., Fan, J., Li, Z., Chen, Q., Zhai, P., Dai, Z., and Li, X.: Precipitation and air pollution
956   at mountain and plain stations in northern China: Insights gained from observations and modeling,
957   Journal of Geophysical Research: Atmospheres, 119, 4793-4807, 10.1002/2013JD021161, 2014.

958 Guo, J., Deng, M., Lee, S. S., Wang, F., Li, Z., Zhai, P., Liu, H., Lv, W., Yao, W., and Li, X.: Delaying
959   precipitation and lightning by air pollution over the Pearl River Delta. Part I: Observational analyses,
960   Journal of Geophysical Research: Atmospheres, 121, 6472-6488, 10.1002/2015jd023257, 2016.

961 Guo, J., Su, T., Li, Z., Miao, Y., Li, J., Liu, H., Xu, H., Cribb, M., and Zhai, P.: Declining frequency of
962   summertime local-scale precipitation over eastern China from 1970 to 2010 and its potential link to
963   aerosols, Geophysical Research Letters, 44, 5700-5708, 10.1002/2017gl073533, 2017.

964 Guo, J., Liu, H., Li, Z., Rosenfeld, D., Jiang, M., Xu, W., Jiang, J. H., He, J., Chen, D., Min, M., and
965   Zhai, P.: Aerosol-induced changes in the vertical structure of precipitation: a perspective of TRMM
966   precipitation radar, Atmos. Chem. Phys., 18, 13329-13343, 10.5194/acp-18-13329-2018, 2018.

967 Haralick, R. M., Shanmugam, K., and Dinstein, I.: Textural Features for Image Classification, IEEE
968   Transactions on Systems, Man, and Cybernetics, SMC-3, 610-621, 10.1109/TSMC.1973.4309314,
969   1973.

970 Haralick, R. M.: Statistical and structural approaches to texture, Proceedings of the IEEE, 67, 786-804,
971   10.1109/PROC.1979.11328, 1979.

972 Houze Jr., R. A.: Orographic effects on precipitating clouds, Reviews of Geophysics, 50,
973   10.1029/2011rg000365, 2012.

974 Houze Jr., R. A.: Cloud dynamics, Academic press, 2014.

975 Jiang, J. H., Su, H., Huang, L., Wang, Y., Massie, S. T., Zhao, B., Omar, A., and Wang, Z.: Contrasting
976   effects on deep convective clouds by different types of aerosols, Nature Communications, 9, 7,
977   10.1038/s41467-018-06280-4, 2018.

978 Jiang, Y., Liu, X., Yang, X.-Q., and Wang, M.: A numerical study of the effect of different aerosol types
979   on East Asian summer clouds and precipitation, Atmospheric Environment, 70, 51-63,
980   https://doi.org/10.1016/j.atmosenv.2012.12.039, 2013.

981 Kaufman, Y. J., and Nakajima, T.: EFFECT OF AMAZON SMOKE ON CLOUD MICROPHYSICS
982   AND ALBEDO - ANALYSIS FROM SATELLITE IMAGERY, Journal of Applied Meteorology,
983   32, 729-744, 10.1175/1520-0450(1993)032<0729:eoasoc>2.0.co;2, 1993.

984 Kaufman, Y. J., Tanre, D., and Boucher, O.: A satellite view of aerosols in the climate system, Nature,
985   419, 215-223, 10.1038/nature01091, 2002.

986 Kaufman, Y. J., Koren, I., Remer, L. A., Rosenfeld, D., and Rudich, Y.: The effect of smoke, dust, and
987   pollution aerosol on shallow cloud development over the Atlantic Ocean, Proceedings of the
988   National Academy of Sciences, 102, 11207-11212, 10.1073/pnas.0505191102, 2005.

989 Khain, A., Rosenfeld, D., and Pokrovsky, A.: Aerosol impact on the dynamics and microphysics of deep
990   convective clouds, Quarterly Journal of the Royal Meteorological Society, 131, 2639-2663,
991   10.1256/qj.04.62, 2005.

992 Kirshbaum, D. J., and Durran, D. R.: Factors Governing Cellular Convection in Orographic Precipitation,
993   Journal of the Atmospheric Sciences, 61, 682-698, 10.1175/1520-
994   0469(2004)061<0682:fgccio>2.0.co;2, 2004.

995 Kirshbaum, D. J., and Durran, D. R.: Atmospheric Factors Governing Banded Orographic Convection,
996   Journal of the Atmospheric Sciences, 62, 3758-3774, 10.1175/jas3568.1, 2005.

997 Kirshbaum, D. J., Bryan, G. H., Rotunno, R., and Durran, D. R.: The Triggering of Orographic Rainbands

by Small-Scale Topography, Journal of the Atmospheric Sciences, 64, 1530-1549, 10.1175/jas3924.1, 2007.

Koren, I., Kaufman, Y. J., Remer, L. A., and Martins, J. V.: Measurement of the effect of Amazon smoke on inhibition of cloud formation, Science, 303, 1342-1345, 10.1126/science.1089424, 2004.

Koren, I., Kaufman, Y. J., Rosenfeld, D., Remer, L. A., and Rudich, Y.: Aerosol invigoration and restructuring of Atlantic convective clouds, Geophysical Research Letters, 32, L14828, 10.1029/2005gl023187, 2005.

Koren, I., Martins, J. V., Remer, L. A., and Afargan, H.: Smoke invigoration versus inhibition of clouds over the Amazon, Science, 321, 946-949, 10.1126/science.1159185, 2008.

Koren, I., Feingold, G., and Remer, L. A.: The invigoration of deep convective clouds over the Atlantic: aerosol effect, meteorology or retrieval artifact?, Atmos. Chem. Phys., 10, 8855-8872, 10.5194/acp-10-8855-2010, 2010.

Li, W., Luo, C., Wang, D., and Lei, T.: Diurnal variations of precipitation over the South China Sea, Meteorology and Atmospheric Physics, 109, 33-46, 10.1007/s00703-010-0094-8, 2010.

Li, Z. and D. Weng.: A computer model to determine topographic parameters, Acta Geographica Sinica, 42, 269-278, 10.11821/xb198703009, 1987.

Li, Z., and D. Weng.: A computer model for calculating the duration of sunshine in mountainous areas, Chinese Science Bulletin, 33, 1624-1627, CNKI:SUN:JXTW.0.1988-19-011, 1988.

Li, Z., and D. Weng.: A numerical model for hilly-land global radiation, Acta Meteorologica Sinica, 3, 661-668, CNKI:SUN:QXXW.0.1989-05-010, 1989.

Li, Z., Zhao, X., Kahn, R., Mishchenko, M., Remer, L., Lee, K.-H., M.Wang, Laszlo, I., Nakajima, T., and Maring, H.: Uncertainties in satellite remote sensing of aerosols and impact on monitoring its long-term trend: a review and perspective, Annales Geophysicae, 27, 2755-2770, 10.5194/angeo-27-2755-2009, 2009.

Li, Z., Niu, F., Fan, J., Liu, Y., Rosenfeld, D., and Ding, Y.: Long-term impacts of aerosols on the vertical development of clouds and precipitation, Nature Geoscience, 4, 888-894, 10.1038/ngeo1313, 2011.

Li, Z., Lau, W. K. M., Ramanathan, V., Wu, G., Ding, Y., Manoj, M. G., Liu, J., Qian, Y., Li, J., Zhou, T., Fan, J., Rosenfeld, D., Ming, Y., Wang, Y., Huang, J., Wang, B., Xu, X., Lee, S. S., Cribb, M., Zhang, F., Yang, X., Zhao, C., Takemura, T., Wang, K., Xia, X., Yin, Y., Zhang, H., Guo, J., Zhai, P. M., Sugimoto, N., Babu, S. S., and Brasseur, G. P.: Aerosol and monsoon climate interactions over Asia, Reviews of Geophysics, 54, 866-929, 10.1002/2015rg000500, 2016.

Li, Z., Wang, Y., Guo, J., Zhao, C., Cribb, M. C., Dong, X., Fan, J., Gong, D., Huang, J., Jiang, M., Jiang, Y., Lee, S.-S., Li, H., Li, J., Liu, J., Qian, Y., Rosenfeld, D., Shan, S., Sun, Y., Wang, H., Xin, J., Yan, X., Yang, X., Yang, X.-q., Zhang, F., and Zheng, Y.: East Asian Study of Tropospheric Aerosols and their Impact on Regional Clouds, Precipitation, and Climate (EAST-AIRCPC), Journal of Geophysical Research-Atmospheres, 124, 10.1029/2019jd030758, 2019.

Lima, M. A., and Wilson, J. W.: Convective Storm Initiation in a Moist Tropical Environment, Monthly Weather Review, 136, 1847-1864, 10.1175/2007mwr2279.1, 2008.

Liu, J., and Li, Z.: Estimation of cloud condensation nuclei concentration from aerosol optical quantities: influential factors and uncertainties, Atmos. Chem. Phys., 14, 471-483, 10.5194/acp-14-471-2014, 2014.

Lohmann, U., and Feichter, J.: Global indirect aerosol effects: a review, Atmos. Chem. Phys., 5, 715-737, 10.5194/acp-5-715-2005, 2005.

设置了格式: 字体: (默认) Times New Roman

Lynn, B., Khain, A., Rosenfeld, D., and Woodley, W. L.: Effects of aerosols on precipitation from orographic clouds, Journal of Geophysical Research: Atmospheres, 112, 10.1029/2006jd007537, 2007.

McCormick, R. A., and Ludwig, J. H.: Climate Modification by Atmospheric Aerosols, Science, 156, 1358-1359, 10.1126/science.156.3780.1358, 1967.

Mecikalski, J. R., and Bedka, K. M.: Forecasting convective initiation by monitoring the evolution of moving cumulus in daytime GOES imagery, Monthly Weather Review, 134, 49-78, 10.1175/mwr3062.1, 2006.

Meskhidze, N., Remer, L. A., Platnick, S., Negrón Juárez, R., Lichtenberger, A. M., and Aiyyer, A. R.: Exploring the differences in cloud properties observed by the Terra and Aqua MODIS Sensors, Atmos. Chem. Phys., 9, 3461-3475, 10.5194/acp-9-3461-2009, 2009.

Niu, F., and Li, Z.: Systematic variations of cloud top temperature and precipitation rate with aerosols over the global tropics, Atmospheric Chemistry and Physics, 12, 8491-8498, 10.5194/acp-12-8491-2012, 2012.

Purdom, J. F. W.: Some Uses of High-Resolution GOES Imagery in the Mesoscale Forecasting of Convection and Its Behavior, Monthly Weather Review, 104, 1474-1483, 10.1175/1520-0493(1976)104<1474:suohrg>2.0.co;2, 1976.

Qiu, Y., Zhao, C., Guo, J., and Li, J.: 8-Year ground-based observational analysis about the seasonal variation of the aerosol-cloud droplet effective radius relationship at SGP site, Atmospheric Environment, 164, 139-146, https://doi.org/10.1016/j.atmosenv.2017.06.002, 2017.

Ramanathan, V., Crutzen, P. J., Kiehl, J. T., and Rosenfeld, D.: Aerosols, Climate, and the Hydrological Cycle, Science, 294, 2119-2124, 10.1126/science.1064034, 2001.

Redelsperger, J.-L., Parsons, D. B., and Guichard, F.: Recovery Processes and Factors Limiting Cloud-Top Height following the Arrival of a Dry Intrusion Observed during TOGA COARE, Journal of the Atmospheric Sciences, 59, 2438-2457, 10.1175/1520-0469(2002)059<2438:rpaflc>2.0.co;2, 2002.

Roe, G. H.: OROGRAPHIC PRECIPITATION, Annual Review of Earth and Planetary Sciences, 33, 645-671, 10.1146/annurev.earth.33.092203.122541, 2005.

Romatschke, U., and Jr., R. A. H.: Extreme Summer Convection in South America, Journal of Climate, 23, 3761-3791, 10.1175/2010jcli3465.1, 2010.

Romatschke, U., Medina, S., and Jr., R. A. H.: Regional, Seasonal, and Diurnal Variations of Extreme Convection in the South Asian Region, Journal of Climate, 23, 419-439, 10.1175/2009jcli3140.1, 2010.

Romatschke, U., and Jr., R. A. H.: Characteristics of Precipitating Convective Systems in the South Asian Monsoon, Journal of Hydrometeorology, 12, 3-26, 10.1175/2010jhm1289.1, 2011a.

Romatschke, U., and Jr., R. A. H.: Characteristics of Precipitating Convective Systems in the Premonsoon Season of South Asia, Journal of Hydrometeorology, 12, 157-180, 10.1175/2010jhm1311.1, 2011b.

Rosenfeld, D.: Suppression of Rain and Snow by Urban and Industrial Air Pollution, Science, 287, 1793-1796, 10.1126/science.287.5459.1793, 2000.

Rosenfeld, D., and Givati, A.: Evidence of Orographic Precipitation Suppression by Air Pollution–Induced Aerosols in the Western United States, Journal of Applied Meteorology and Climatology, 45, 893-911, 10.1175/jam2380.1, 2006.

Rosenfeld, D., Lohmann, U., Raga, G. B., O'Dowd, C. D., Kulmala, M., Fuzzi, S., Reissell, A., and

Andreae, M. O.: Flood or Drought: How Do Aerosols Affect Precipitation?, Science, 321, 1309-1313, 10.1126/science.1160606, 2008.

Rosenfeld, D., and Ulrike Lohmann, G. B. R., Colin D. O'Dowd, Markku Kulmala, Sandro Fuzzi, Anni Reissell, Meinrat O. Andreae: Flood or Drought: How Do Aerosols Affect Precipitation?, Science, 321, 1309-1313, 10.1126/science.1160606, 2008.

Rosenfeld, D., Andreae, M. O., Asmi, A., Chin, M., de Leeuw, G., Donovan, D. P., Kahn, R., Kinne, S., Kivekäs, N., Kulmala, M., Lau, W., Schmidt, K. S., Suni, T., Wagner, T., Wild, M., and Quaas, J.: Global observations of aerosol-cloud-precipitation-climate interactions, Reviews of Geophysics, 52, 1-59, 10.1002/2013rg000441, 2014a.

Rosenfeld, D., Sherwood, S., Wood, R., and Donner, L. J.: Climate Effects of Aerosol-Cloud Interactions, Science, 343, 379-380, 10.1126/science.1247490, 2014b.

Rosenfeld, D., Jin Dai, Xing Yu, Zhanyu Yao, Xiaohong Xu, Xing Yang, Chuanli Du: Inverse Relations Between Amounts of Air Pollution and Orographic Precipitation, Science, 315, 1396-1398, 10.1126/science.1137949, 2007.

Rossow, W. B., and Schiffer, R. A.: ISCCP Cloud Data Products, 10.1175/1520-0477(1991)0722.0.CO;2, 1991.

Stevens, B., and Feingold, G.: Untangling aerosol effects on clouds and precipitation in a buffered system, Nature, 461, 607, 10.1038/nature08281, 2009.

Sui, C.-H., Lau, K.-M., Takayabu, Y. N., and Short, D. A.: Diurnal Variations in Tropical Oceanic Cumulus Convection during TOGA COARE, Journal of the Atmospheric Sciences, 54, 639-655, 10.1175/1520-0469(1997)054<0639:dvitoc>2.0.co;2, 1997.

Tao, W. K., Chen, J. P., Li, Z. Q., Wang, C., and Zhang, C. D.: Impact of aerosols on convective clouds and precipitation, Reviews of Geophysics, 50, 10.1029/2011rg000369, 2012.

Twomey, S., and Warner, J.: Comparison of Measurements of Cloud Droplets and Cloud Nuclei, Journal of the Atmospheric Sciences, 24, 702-703, 10.1175/1520-0469(1967)024<0702:comocd>2.0.co;2, 1967.

Twomey, S.: Pollution and the planetary albedo, Atmospheric Environment (1967), 8, 1251-1256, https://doi.org/10.1016/0004-6981(74)90004-3, 1974.

Wang, Q., Li, Z., Guo, J., Zhao, C., and Cribb, M.: The climate impact of aerosols on the lightning flash rate: is it detectable from long-term measurements?, Atmospheric Chemistry and Physics, 18, 12797-12816, 10.5194/acp-18-12797-2018, 2018.

Wang, Y., Khalizov, A., Levy, M., and Zhang, R.: New Directions: Light absorbing aerosols and their atmospheric impacts, Atmospheric Environment, 81, 713-715, 10.1016/j.atmosenv.2013.09.034, 2013.

Welch, R. M., Kuo, K. S., Wielicki, B. A., Sengupta, S. K., and Parker, L.: Marine Stratocumulus Cloud Fields off the Coast of Southern California Observed Using LANDSAT Imagery. Part I: Structural Characteristics, Journal of Applied Meteorology, 27, 341-362, 10.1175/1520-0450(1988)027<0341:mscfot>2.0.co;2, 1988a.

Welch, R. M., Sengupta, S. K., and Chen, D. W.: Cloud field classification based upon high spatial resolution textural features: 1. Gray level co-occurrence matrix approach, Journal of Geophysical Research: Atmospheres, 93, 12663-12681, 10.1029/JD093iD10p12663, 1988b.

Welch, R. M., Sengupta, S. K., and Kuo, K. S.: Marine Stratocumulus Cloud Fields off the Coast of Southern California Observed Using LANDSAT Imagery. Part II: Textural Analysis, Journal of

1127   Applied Meteorology, 27, 363-378, 10.1175/1520-0450(1988)027<0363:mscfot>2.0.co;2, 1988c.

1128 Wielicki, B. A., and Welch, R. M.: Cumulus Cloud Properties Derived Using LANDSAT Satellite Data,
1129   Journal of Climate and Applied Meteorology, 25, 261-276, 10.1175/1520-
1130   0450(1986)025<0261:ccpdul>2.0.co;2, 1986.

1131 Williams, E., Rosenfeld, D., Madden, N., Gerlach, J., Gears, N., Atkinson, L., Dunnemann, N., Frostrom,
1132   G., Antonio, M., Biazon, B., Camargo, R., Franca, H., Gomes, A., Lima, M., Machado, R., Manhaes,
1133   S., Nachtigall, L., Piva, H., Quintiliano, W., Machado, L., Artaxo, P., Roberts, G., Renno, N.,
1134   Blakeslee, R., Bailey, J., Boccippio, D., Betts, A., Wolff, D., Roy, B., Halverson, J., Rickenbach, T.,
1135   Fuentes, J., and Avelino, E.: Contrasting convective regimes over the Amazon: Implications for
1136   cloud electrification, Journal of Geophysical Research: Atmospheres, 107, LBA 50-51-LBA 50-19,
1137   doi:10.1029/2001JD000380, 2002.

1138 Williams, M., and Houze Jr., R. A.: Satellite-Observed Characteristics of Winter Monsoon Cloud Clusters,
1139   Monthly Weather Review, 115, 505-519, 10.1175/1520-0493(1987)115<0505:socowm>2.0.co;2,
1140   1987.

1141 Wilson, A. M., Parmentier, B., and Jetz, W.: Systematic land cover bias in Collection 5 MODIS cloud
1142   mask and derived products — A global overview, Remote Sensing of Environment, 141, 149-154,
1143   https://doi.org/10.1016/j.rse.2013.10.025, 2014.

1144 Xiao, H., Yin, Y., Jin, L., Chen, Q., and Chen, J.: Simulation of the effects of aerosol on mixed-phase
1145   orographic clouds using the WRF model with a detailed bin microphysics scheme, Journal of
1146   Geophysical Research: Atmospheres, 120, 8345-8358, 10.1002/2014jd022988, 2015.

1147 Yang, G.-Y., and Slingo, J.: The Diurnal Cycle in the Tropics, Monthly Weather Review, 129, 784-801,
1148   10.1175/1520-0493(2001)129<0784:tdcitt>2.0.co;2, 2001.

1149 Yang, X., Zhao, C., Guo, J., and Wang, Y.: Intensification of aerosol pollution associated with its feedback
1150   with surface solar radiation and winds in Beijing, Journal of Geophysical Research-Atmospheres,
1151   121, 4093-4099, 10.1002/2015jd024645, 2016a.

1152 Yang, X., Zhao, C., Zhou, L., Wang, Y., and Liu, X.: Distinct impact of different types of aerosols on
1153   surface solar radiation in China, Journal of Geophysical Research-Atmospheres, 121, 6459-6471,
1154   10.1002/2016jd024938, 2016b.

1155 Yang, X., Zhao, C., Zhou, L., Li, Z., Cribb, M., and Yang, S.: Wintertime cooling and a potential
1156   connection with transported aerosols in Hong Kong during recent decades, Atmospheric Research,
1157   211, 52-61, 10.1016/j.atmosres.2018.04.029, 2018.

1158 Yang, Y., Fan, J., Leung, L. R., Zhao, C., Li, Z., and Rosenfeld, D.: Mechanisms Contributing to
1159   Suppressed Precipitation in Mt. Hua of Central China. Part I: Mountain Valley Circulation, Journal
1160   of the Atmospheric Sciences, 73, 1351-1366, 10.1175/jas-d-15-0233.1, 2016c.

1161 Yang, Y., Zhao, C., Dong, X., Fan, G., Zhou, Y., Wang, Y., Zhao, L., Lv, F., and Yan, F.: Toward
1162   understanding the process-level impacts of aerosols on microphysical properties of shallow cumulus
1163   cloud using aircraft observations, Atmospheric Research, 221, 27-33,
1164   10.1016/j.atmosres.2019.01.027, 2019.

1165 Zhang, F., Ren, J., Fan, T., Chen, L., Xu, W., Sun, Y., Zhang, R., Liu, J., Jiang, S., Jin, X., Wu, H., Li, S.,
1166   Cribb, M. C., and Li, Z.: Significantly Enhanced Aerosol CCN Activity and Number Concentrations
1167   by Nucleation-Initiated Haze Events: A Case Study in Urban Beijing, Journal of Geophysical
1168   Research: Atmospheres, 124, 14102-14113, https://doi.org/10.1029/2019JD031457, 2019.

1169 Zhao, C., Klein, S. A., Xie, S., Liu, X., Boyle, J. S., and Zhang, Y.: Aerosol first indirect effects on non-

precipitating low-level liquid cloud properties as simulated by CAM5 at ARM sites, 39, 10.1029/2012gl051213, 2012.

Zhao, C., and Garrett, T. J.: Effects of Arctic haze on surface cloud radiative forcing, Geophysical Research Letters, 42, 557-564, 10.1002/2014gl062015, 2015.

Zhao, C., Lin, Y., Wu, F., Wang, Y., Li, Z., Rosenfeld, D., and Wang, Y.: Enlarging Rainfall Area of Tropical Cyclones by Atmospheric Aerosols, Geophysical Research Letters, 45, 8604-8611, 10.1029/2018gl079427, 2018a.

Zhao, C., Qiu, Y., Dong, X., Wang, Z., Peng, Y., Li, B., Wu, Z., and Wang, Y.: Negative Aerosol-Cloud re Relationship From Aircraft Observations Over Hebei, China, Earth and Space Science, 5, 19-29, 10.1002/2017ea000346, 2018b.

Zhao, C., Zhao, L., and Dong, X.: A Case Study of Stratus Cloud Properties Using In Situ Aircraft Observations over Huanghua, China, 10, 19, 10.3390/atmos10010019, 2019.

Zhao, C., Yang, Y., Fan, H., Huang, J., Fu, Y., Zhang, X., Kang, S., Cong, Z., Letu, H., and Menenti, M.: Aerosol characteristics and impacts on weather and climate over the Tibetan Plateau, National Science Review, 7, 492-495, 10.1093/nsr/nwz184, 2020.

Zhou, S., Yang, J., Wang, W. C., Zhao, C., Gong, D., and Shi, P.: An observational study of the effects of aerosols on diurnal variation of heavy rainfall and associated clouds over Beijing–Tianjin–Hebei, Atmos. Chem. Phys., 20, 5211-5229, 10.5194/acp-20-5211-2020, 2020.

Zhou, T., Yu, R., Chen, H., Dai, A., and Pan, Y.: Summer Precipitation Frequency, Intensity, and Diurnal Cycle over China: A Comparison of Satellite Data with Rain Gauge Observations, Journal of Climate, 21, 3997-4010, 10.1175/2008jcli2028.1, 2008.

设置了格式: 字体: (默认) Times New Roman

1193 **Figures**

1194
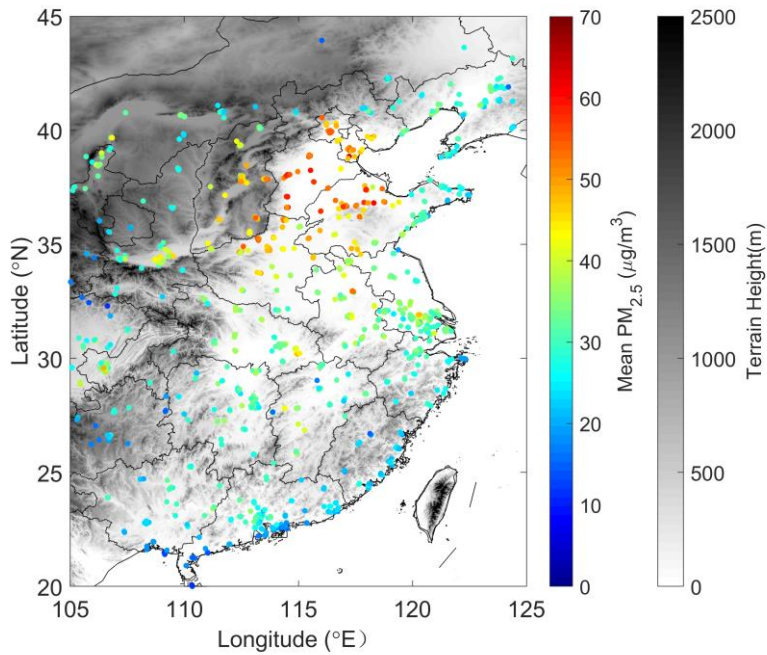
1195 **Figure 1**. Surface elevation and the mean value of ground-based PM$_{2.5}$
1196 measurements over eastern China. The terrain height (TH) of this region is
1197 represented with gray shading. Colored dots show the mean PM$_{2.5}$ concentration
1198 from 1205 surface stations during May-September in 2016-2017 over this area.

1199

1200
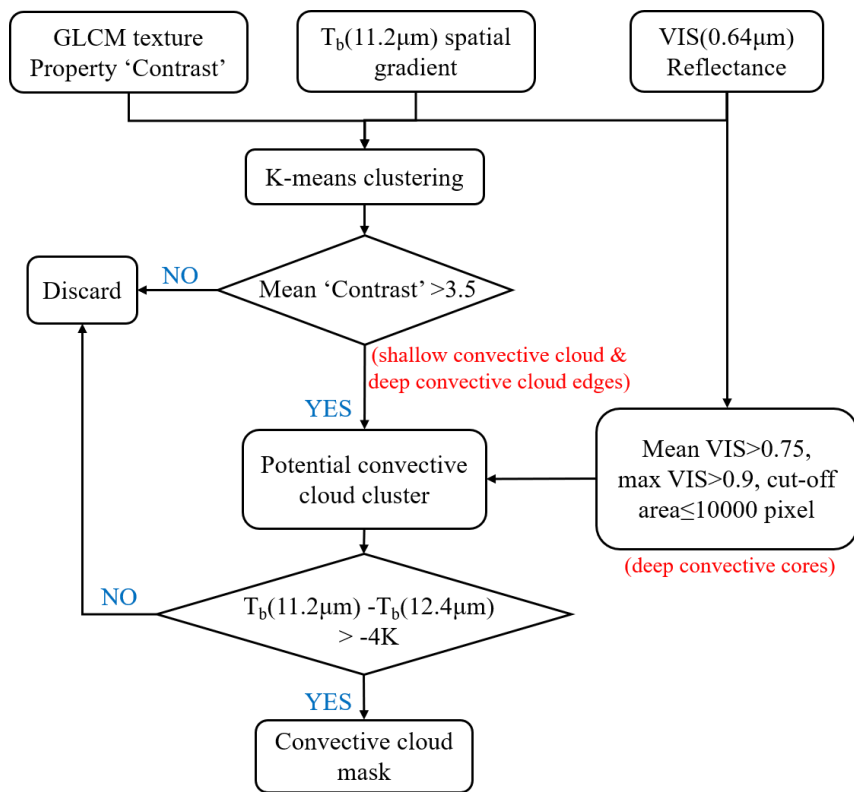
1201   **Figure 2**. Flowchart of the convective cloud identification method.

1202
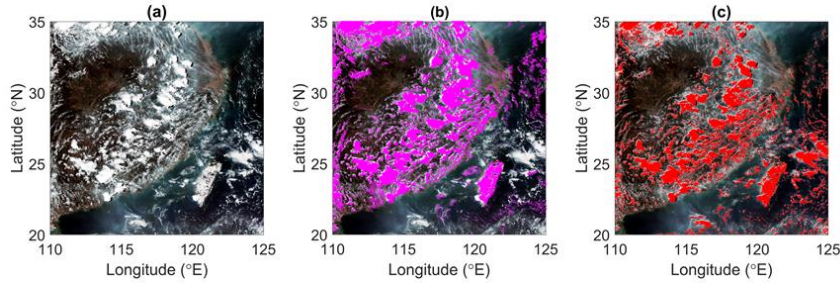
Figure 3. Comparisons between MODIS cloud mask and the cloud identified by our convective cloud (CC) mask, at 13:40 LT on July 30th, 2016 and 14:20 LT on June 22nd, 2016. (a, d) The true color image, (b, e) MODIS cloud mask data from the MYD35 product (magenta points), and (c, f) convective clouds (CC) identified using the TCT-CID method.

1214

1215

1216
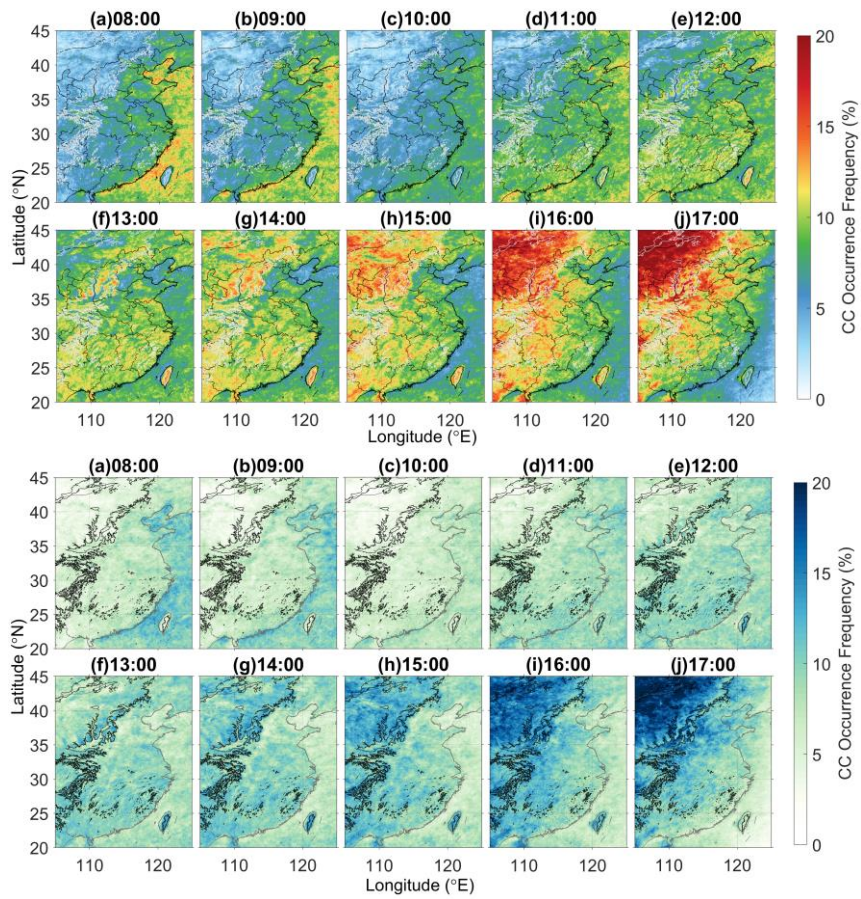
1217 **Figure 4**. Diurnal cycle of convective cloud (CC) occurrence frequency (OF) during

1218 daytime. The gray contour lines in each figure represent the terrain height (TH) at 1000

1219 m. Most locations west of the contour line have TH >1000 m, whereas terrain east of

1220 the contour lines has TH <1000 m.

1221

1222

1223
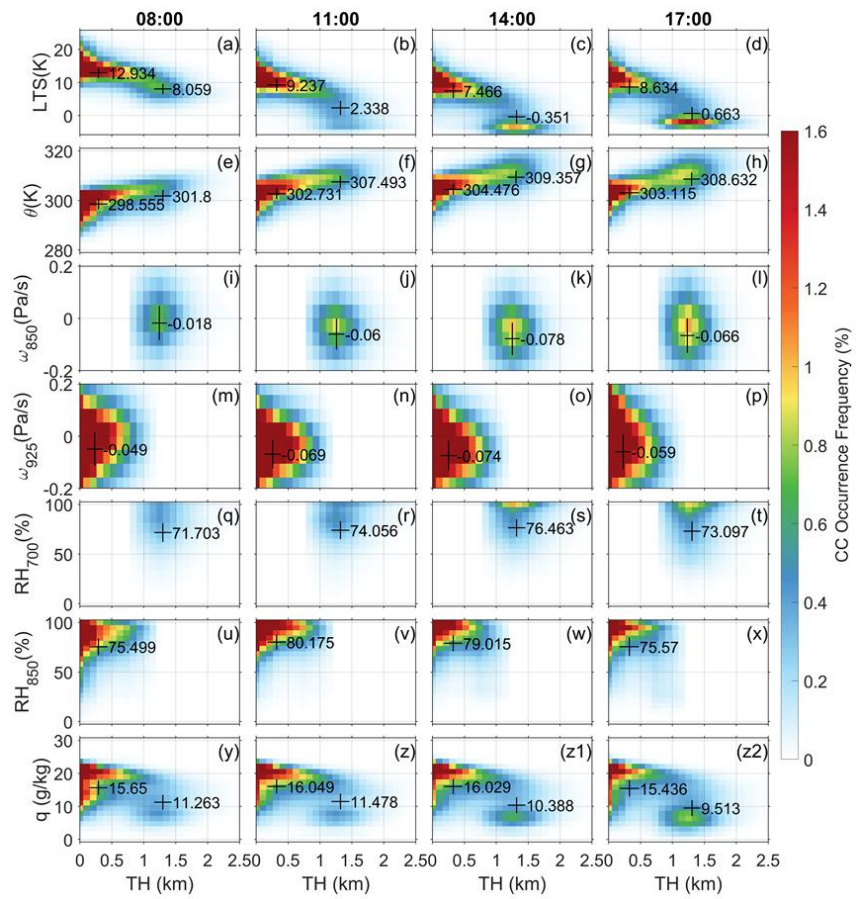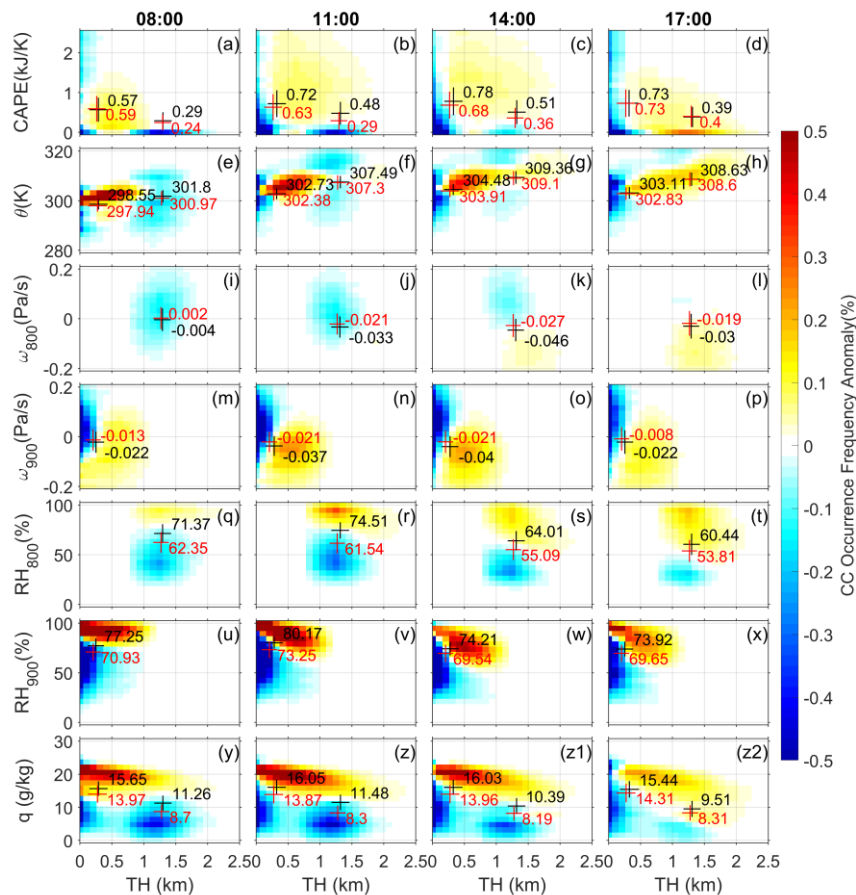
Figure 5. Over-land convective cloud occurrence frequency(CC OF) anomaly with respect to terrain height (TH) and (a-d) convective available potential energy (CAPE), (e-h) potential temperature (θ), (i-l) vertical pressure velocity at 800 hPa (ω_{800}) over terrain above 1000 m, (m-p) vertical pressure velocity at 900 hPa (ω_{900}) over terrain below 1000 m, (q-t) relative humidity at 800 hPa (RH_{800}) over terrain above 1000 m, (u-x) relative humidity at 900 hPa (RH_{900}) over terrain below 1000 m, (y-z2) specific humidity at 2m (q). The columns represent local time over the ROI of 08:00, 11:00, 14:00 and 17:00, respectively. Black (red) crosses and numbers beside mark the mean values of the variables with convective cloud (under all-sky conditions) over regions

1233 with terrain height below 1000 m and above 1000 m, crosses mark the standard

1234 deviations of the variables. Grid points are plotted only if they exceed the 95%

1235 significance level ($p < 0.05$) according to the Pearson's χ^2 test.

1236 –

1237

1238
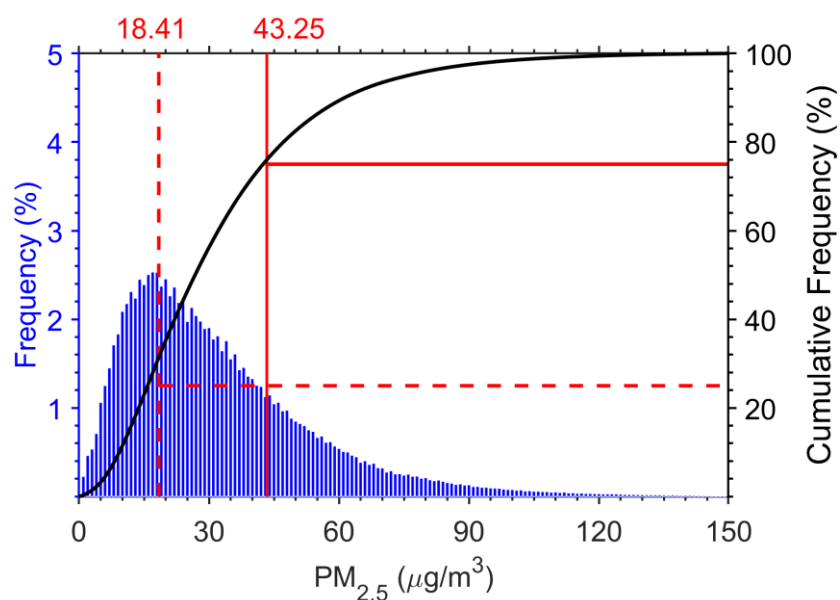
Figure 6. Mean PM$_{2.5}$ concentration distribution for 1205 sites over Eastern China during daytime (08:00-17:00 local time). Blue bars and the black line show the frequency and cumulative frequency of mean PM$_{2.5}$, respectively. The mean value of the top quarter is marked by the red solid line, and the mean value of the bottom quarter is marked with the red dashed line.

1239
1240
1241
1242
1243

1244

1245
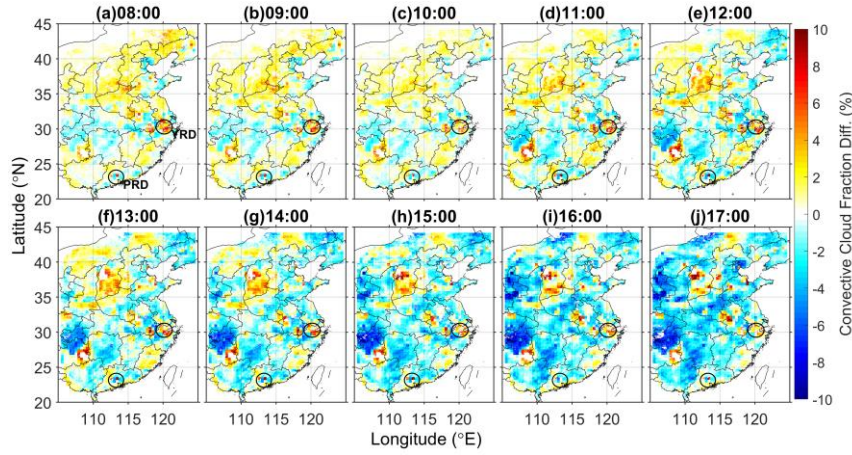
1246 **Figure 7**. Diurnal changes of convective cloud fraction (CCF) difference between
1247 polluted and clean conditions (Polluted-Clean) during May-September in 2016-2017.
1248 Time marked above each figure is the local time. Black circles mark the Yangtze River
1249 Delta (YRD) and Pearl River Delta (PRD). (Note that grid points are plotted only if
1250 they exceed the 95% significance level ($p < 0.05$) according to the Pearson's χ^2 test).

1251

1252

1253

1254

1255
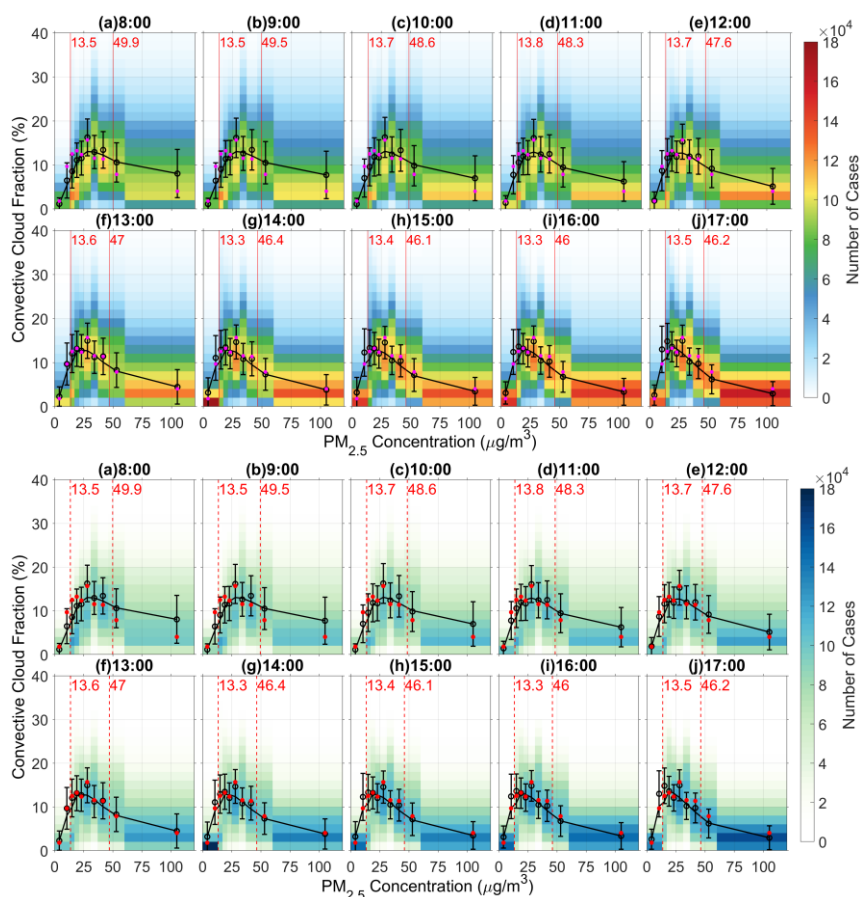
Figure 8. Convective cloud fraction with respect to PM$_{2.5}$ concentration at different times of day during May-September, 2016-2017. Color shading indicates the number of cases corresponding to each specific convective cloud fraction (CCF) and PM$_{2.5}$ bin. Note that PM$_{2.5}$ is separated into ten equal-sample bins. Black circles and error bars are the mean values and standard deviations of CCF in each PM$_{2.5}$ bin within each hour, red dots indicate the mean CCF over all times. Black solid lines represent the three-point moving average of the black circles. Red dashed lines (with red numbers) mark the mean polluted and clean thresholds during each hour.

1264
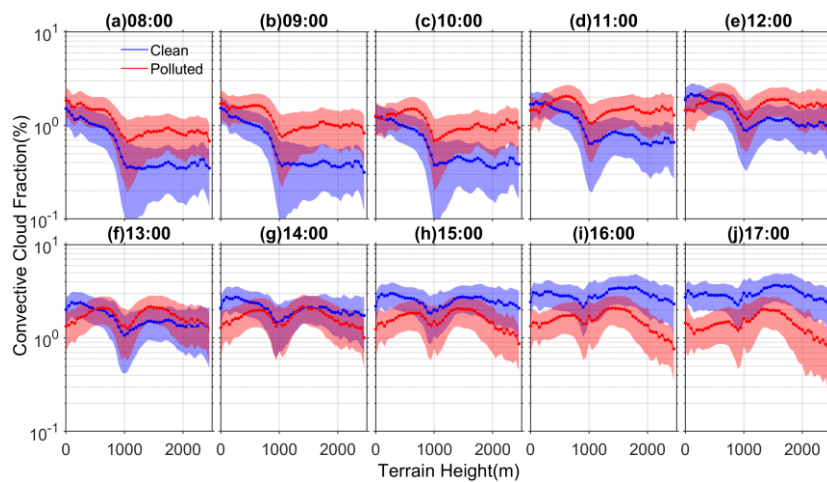
Figure 9. Convective cloud fraction (CCF) normalized by the total number of cases with respect to terrain height changes during May-September, 2016-2017. Data for polluted conditions are plotted in red, whereas those for clean conditions are shown in blue. Solid line and shaded parts are the mean values and standard deviations of the fractions in each TH bin. Dots are plotted only if the difference between clean and polluted cases exceed the 95% significance level ($p < 0.05$) according to the student's t test.

1276

1277

1278
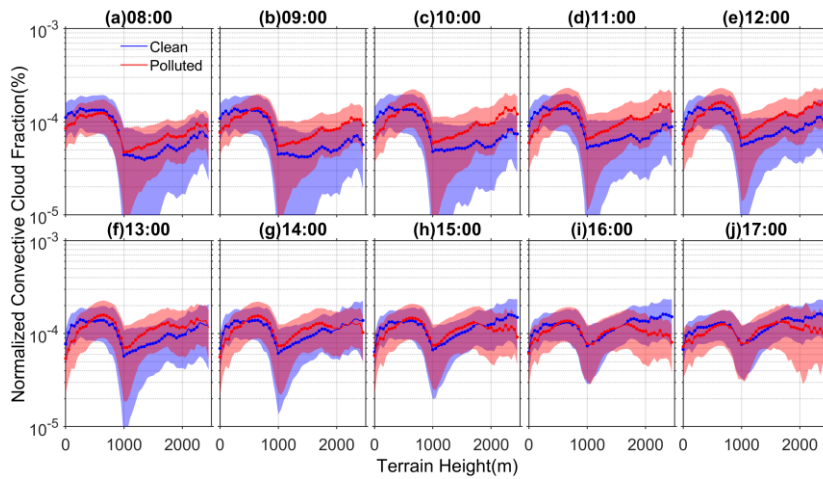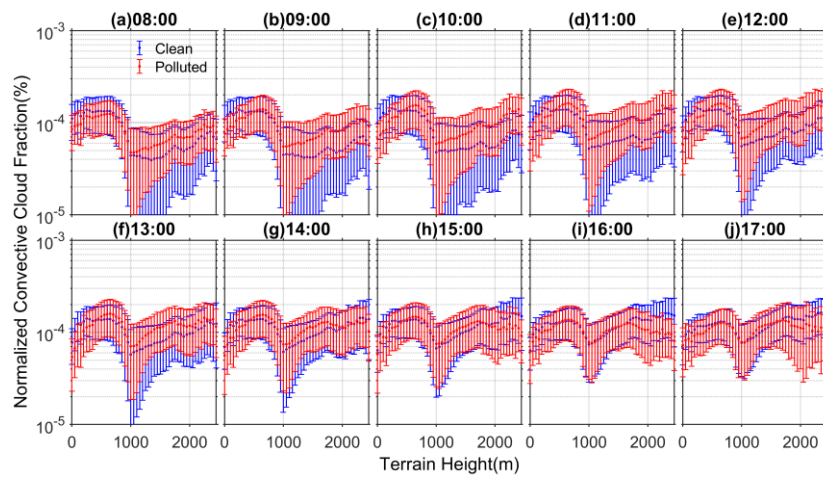
Figure 10. Same as Figure 9, but for CCF that is normalized by the number of cases under polluted and clean conditions during each hour, respectively (Equation 4).

1281

1282

1283
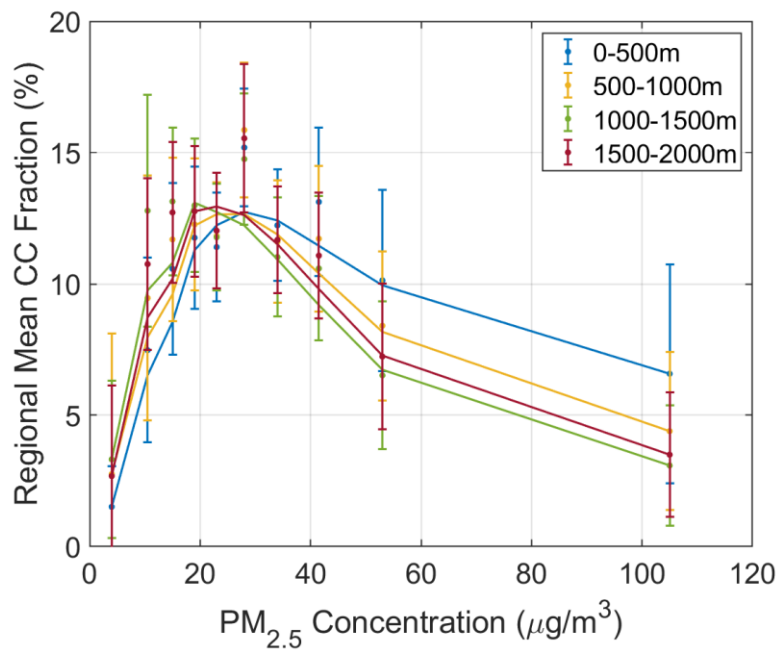
1284 **Figure 11** Convective cloud fraction (CCF) over regions with terrain heights in the

1285 range 0-500 m (blue), 500-1000 m (yellow), 1000-1500 m (green) and 1500-2000 m

1286 (red) with respect to PM$_{2.5}$ concentration during May-September, 2016-2017. Ten

1287 equally sampled PM$_{2.5}$ bins are defined for each terrain height range. The standard

1288 deviations are shown as error bars. Each solid line represents the three-point moving

1289 average for dots in the corresponding color.

1290

1291
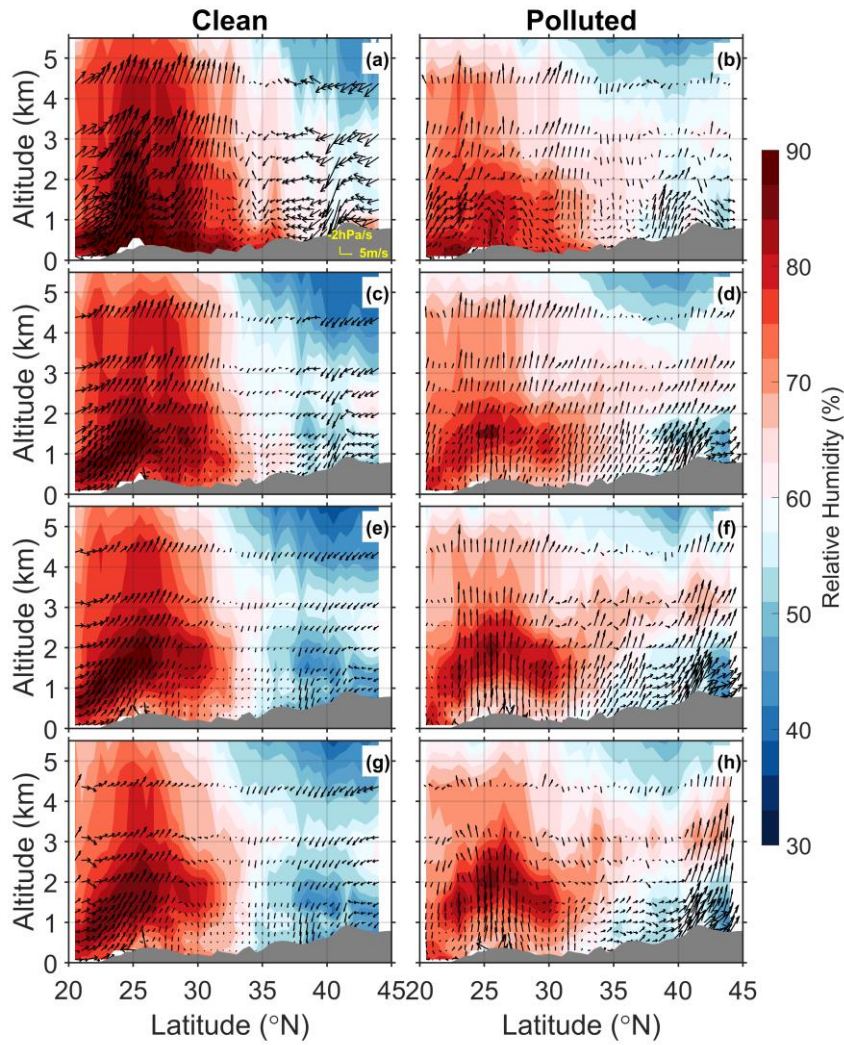
Figure 12. Latitude-altitude cross-sections of mean relative humidity (color-shaded) and mean meridional-vertical wind (vectors) over the continent, averaged along 105 to 125°E for clean (left panel) and polluted (right panel) conditions at (a, b) 08:00 LT, (c, d) 11:00 LT, (e, f) 14:00 LT and (g, h) 17:00 LT during May-September from 2016 to

1296   2017. Vectors are constructed from the easterly wind (u) and vertical velocity (ω),

1297   scaled with -100. Gray shaded parts are the meridional mean terrain heights within ROI.

1298

1299
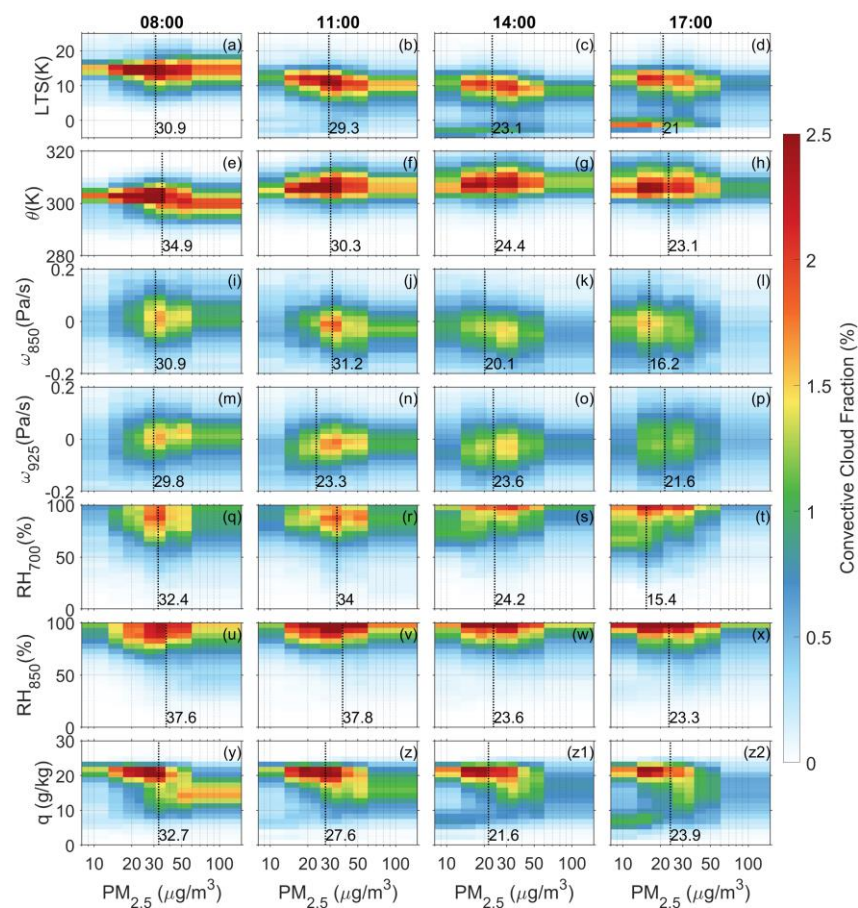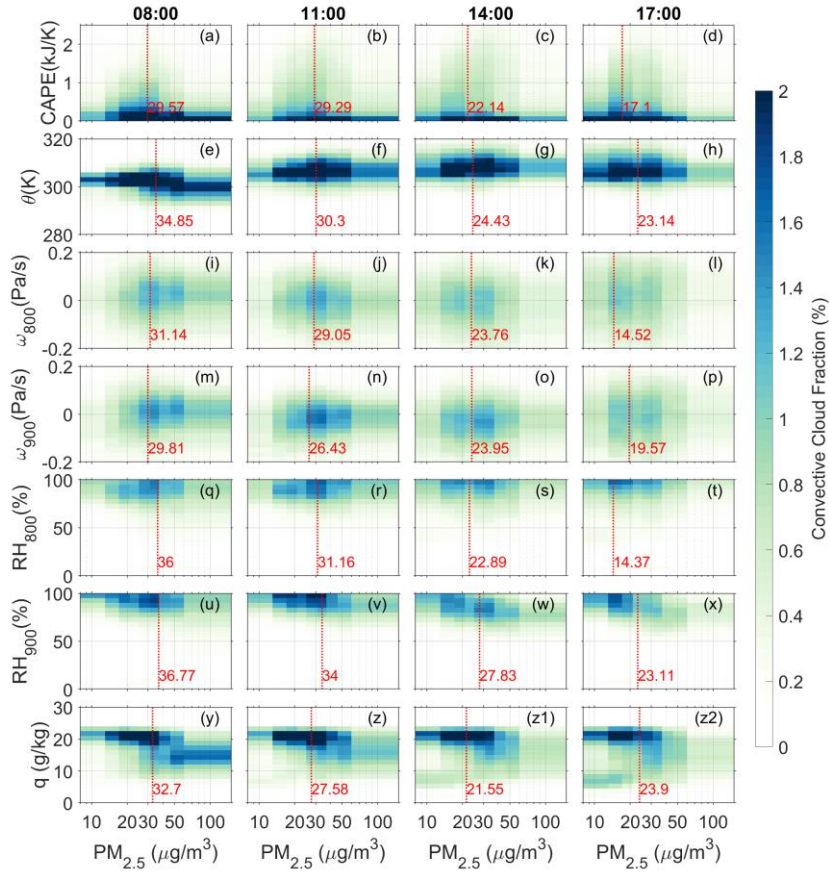
Figure 13. The joint distribution of convective cloud fraction (CCF) with respect to PM$_{2.5}$ concentration and (a-d) lower-tropospheric stability (LTS), (e-h) potential temperature (θ), (i-l) vertical pressure velocity at 800 hPa (ω_{800}) over terrain above 1000 m, (m-p) vertical pressure velocity at 900 hPa (ω_{900}) over terrain below 1000 m, (q-t), relative humidity at 800 hPa (RH$_{800}$) over terrain above 1000 m, (u-x) relative humidity at 900 hPa (RH$_{900}$) over terrain below 1000 m, (y-z2) relative humidity at the surface (RH$_{surface}$). Each column represents a different local time during the day within the ROI, specifically at 08:00, 11:00, 14:00 and 17:00. Black dashed lines and the numbers

1309   beside mark the mean tipping points of CCF at different thermodynamic, dynamical

1310   and humidity levels. Note that x-axis is in log scale.

1311

1312
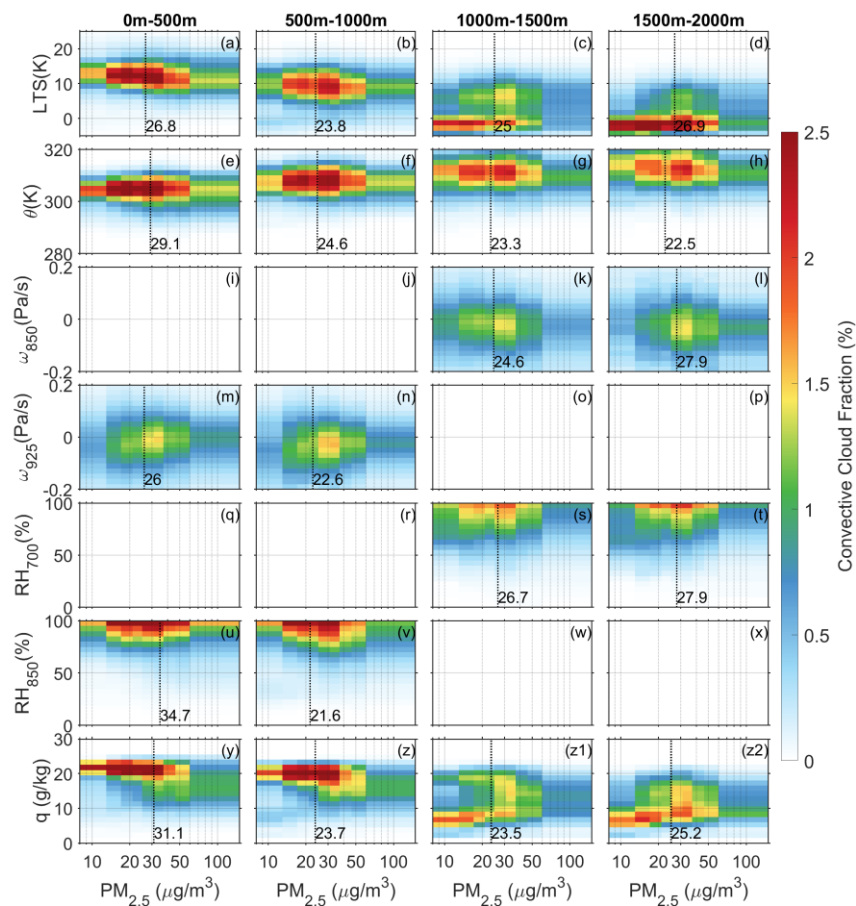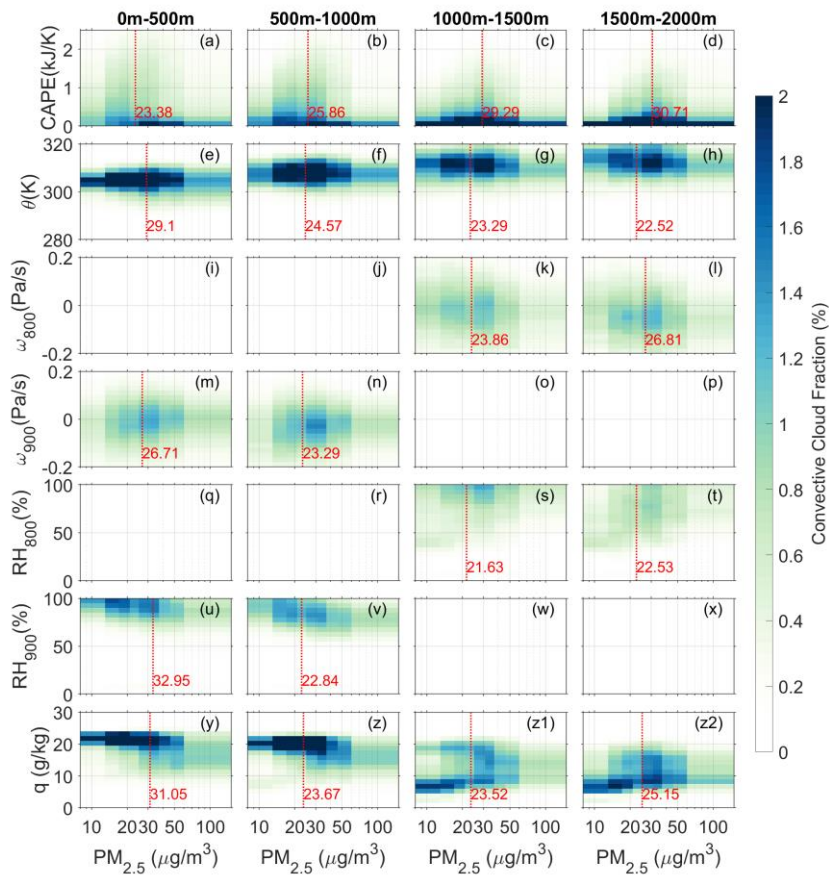
Figure 14. Same as Figure 13, but for different terrain heights; each column represents
a different terrain height range.

1313

1314

1315

1316